The temperature dependence of the elasticity of giant lipid vesicles: An Optical Tweezers, Calorimetry and Confocal Microscopy study

Marie Domange Jordö

Master thesis
Experimental Biomolecular Physics
Department of Applied Physics
The Royal Institute of Technology (KTH)
Stockholm
February 2007

Abstract

It is now widely accepted that domain formation may occur in lipid membranes, especially at the main phase transition were different phases coexist. Using fluorescence confocal microscopy we were able to visualize them. We wanted to investigate a possible correlation between the elasticity and the thermodynamic phase behavior of a phospholipid membrane as well as the domain formation. We chose to study giant unilamellar vesicles (GUVs) made from a 1,2-Dimyristoyl-sn-Glycero-3-Phosphocholine (DMPC) / 1,2-Dipalmitoyl-sn-Glycero-3-Phosphocholine (DPPC) binary mixture. In an optical tweezers set up these approximately 30 μm big vesicles deformed for output laser powers of less then 300 mW. We observed that for a given laser power the same vesicle showed much larger deformations at temperatures corresponding to the main phase transition, than at temperatures just below or above. By quantifying the deformations that occurred as a function of temperature and laser power, we could compare them to heat capacity profiles obtained by differential scanning calorimetry. Our findings fit quite well to the theory that lipid membranes become softer in the main phase transition due to lipids rearranging more easily between the different phases, in our case solid-ordered and liquid -disordered. The lipid membrane being directly affected by the focused laser beam also rises the question of the actual effect of optical tweezers on biological samples, even in the near-infrared and infrared region that is considered relatively harmless. The first part of the discussion will be dedicated to this question, whereas we in the second part will discuss the elastic properties of lipid bilayers, their role in biological processes and the existence or not of a threshold value of the laser power. We will also make an outlook on possible further investigations.

Acknowledgments

I would like to take this opportunity to thank my two great supervisors. Lene Oddershede for giving me the opportunity to come to the Niels Bohr Institute at Copenhagen University, welcoming me into her lab and believing in me. Thomas Heimburg for introducing me to the fascinating world of lipid membranes and for making me see that I had a nice story to tell. Many thanks to all the nice people in the two labs, especially Tabita Winter and Heiko Seeger who always took the time to help me. Also a huge thanks to Matthias Fidorra who taught me everything I know about vesicle electroformation and made my stay in Odense both hardworking and fun. Thanks to the B-floor people who lured me out of the elevator on my way from the basement to the E-floor for well needed and highly enjoyable breaks. Thanks to my family and my friends who bared with me both through the tough times and my sometimes endless rambling about how beautiful giant lipid vesicles are. Thanks to Anna Andersson who gave me the idea of going to Copenhagen. Thanks to Giovanna Russo who took great care of me during my first weeks there and made me feel at home and also to Liselotte Jauffred for welcoming me into her home during my last weeks of stay and my data analysis visits. I would also like to thank the Memphys group at SDU in Odense for having me as a guest and helping me with the sample holder. And finally, last but not least, thanks to my Swedish supervisor at KTH Jerker Widengren for his patience with my endless writing.

Contents

1 Introduction

1.1 What is a lipid membrane?

Lipids can have various structures, head groups sizes, chain lengths and charges making them the chemically most diverse group of molecules in cells. In this introduction we will concentrate on polar lipids. They have a hydrophilic head group and a hydrophobic tail. The two are connected by a a glycerol and in the case of phospholipids also a phosphate PO_4. The tail is composed of two hydrocarbon chains (fatty acid chains) that are not necessarily identical.[1][6] In figure 1 and figure 2 we see the structure of the two phospholipids studied in this thesis; 1,2-Dimyristoyl-sn-Glycero-3-Phosphocholine (DMPC) and 1,2-Dipalmitoyl-sn-Glycero-3-Phosphocholine (DPPC). The only differences between DMPC and DPPC is their chain length, 14 respectively 16 carbons, the two fatty acid chains of their tail being equally long with no double bonds.

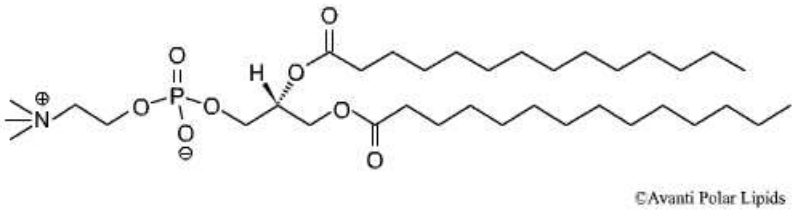

Figure 1: Molecular structure of DMPC

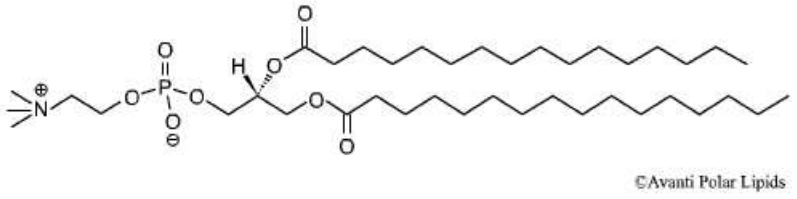

Figure 2: Molecular structure of DPPC

But not all phospholipids use glycerol to bind the head group to the tail. Sphingolipids use the long-chained amine sphingosine instead. The simplest version is ceramide that is a major component in skin cell membranes. Another important lipid in cellular membranes is cholesterol. It has a quite different structure with a steroid ring ended by a little hydrocarbon chain instead of having a fatty acid. It also has a very small head group (-OH).[1]

The amphiphilic nature of polar lipids gives them the property of self-assembling in the presence of water and form 2D and 3D structures. The hydrophobic tails of the lipid molecules are safely tugged away from the surrounding water. The

hydrophobic effect is to a large extent of entropic origin. In the liquid phase water molecules form a loose network of hydrogen bonds that are constantly formed and broken. This network is strongly stabilized by entropy. The hydrocarbon chains of the lipid molecules can't make any hydrogen bonds with the water molecules, so when lipids are put into water the hydrogen bonding network suffers. The formation of aggregates decreases the number of objects in the system and hence reduces its entropy.[2] A certain concentration of lipid molecules is needed for this to occur since it has to be energetically favorable to form clusters. It is referred to as the critical micelle concentration (CMC) or rather the critical aggregation threshold.[6] The type of aggregates that are formed is partly determined by the lipids own molecular shape, for instance if they are cylindrical or cone shaped. This depends on the bulkiness of the head group, the length of the tail and the number of C-C double bonds (degree of saturation). The effective shape of a lipid molecule is described by a packing parameter:

$$P = \frac{v}{al} \tag{1}$$

Figure 3 shows the different types of lipid aggregates that can form and their corresponding packing parameter. v, a and l are defined there as well. Also the temperature plays an important role inducing rotations of the C-C-bonds, thus inducing conformational changes in the hydrocarbon chains. This increases disorder and thereby increases the occupied volume.[3] Especially lipid bilayers and large vesicles are of interest for our study. The more cylindrical the lipids are the more stable the bilayer. If they are not, the monolayers show a spontaneous curvature. If the curvature stress is too high non-lamellar structures form as shown in figure 3. So it is the hydrophobic effect that drives the self-assembly process and the so called spontaneous curvature that decides of the type of the formed structure. It should be noted that the curvature of giant unilamellar vesicles (GUVs) and large liposomes is not due to intrinsic curvature stress. In fact the curvature of vesicles is due to the boundary conditions, the hydrophobic effect forcing the lipid bilayer to close on itself.[3] Worth pointing out is that the mechanisms of self-assembly imply self-healing properties.

Lipid membranes are very thin, of the order of 5 nm since a lipid bilayer only is two molecules thick. There are of course variation due to the conformation and length of the fatty-acid chains or the degree of hydration of the membrane[4]. A typical GUV has a diameter of about 10-30 micrometers. Although membranes are soft materials they are very tough due to hydrophobic forces. Since the lateral mobility of lipids in a liquid membrane is very high, they have no or little resistance to in-plane shearing. The two modes of deformation are bending and stretching/compressing.[7]

The phase of a material reflects it's degree of order. Lipids have two sets of degrees of freedom, positional (translational) and orientational (configurational). The number and type of phases vary depending on the type of lipids present in the membrane. In the case of phospholipids, like the phosphocholines DMPC and DPPC that we are studying, we have a main phase transition between

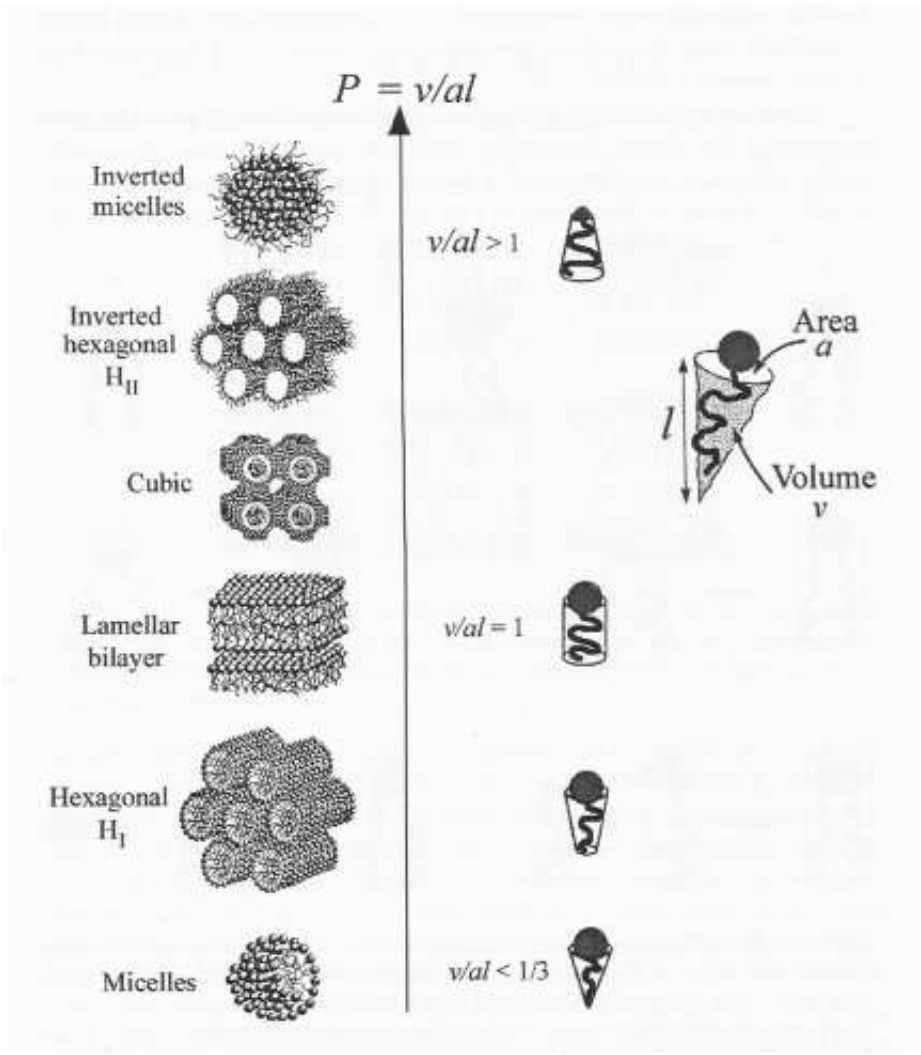

Figure 3: Schematic illustration of lamellar and non-lamellar lipid aggregates formed in water. The different structures have different curvature and are arranged in accordance with the value of packing parameter $P = v/al$.[3]

a solid-ordered and a liquid-disordered phase also called gel and fluid phases. Solid and liquid refer to the positional order degree, i.e. the order in the head groups. Ordered and disordered refer to the orientational order degree, i.e if the fatty acid chains are all oriented in the same direction or if they are bent.[4] Phosphocholines also have a pre-transition that precedes a rippled phase. The conformation of the lipids in this phase is still unclear, but it has been suggested that they are in the solid-ordered phase. The amplitude of the ripple phases increase with chain length.[11] Also lipid mixtures show a phase transition. In the main transition phase coexistence occurs and is believed to give rise to domain formation. For instance in a DMPC/DPPC mixture, the DMPC

having a lower melting temperature will in the transition mainly be in the liquid-disordered phase and the DPPC will mostly be in the solid-ordered phase. The phase transition is in theory a first order transition, but is in practice a much more continuous process with quite strong fluctuations.[4] By integrating heat capacity profiles like the ones shown in figure 4 it is possible to get a measure for the energy that needs to be added in order for the phase transition to take place.

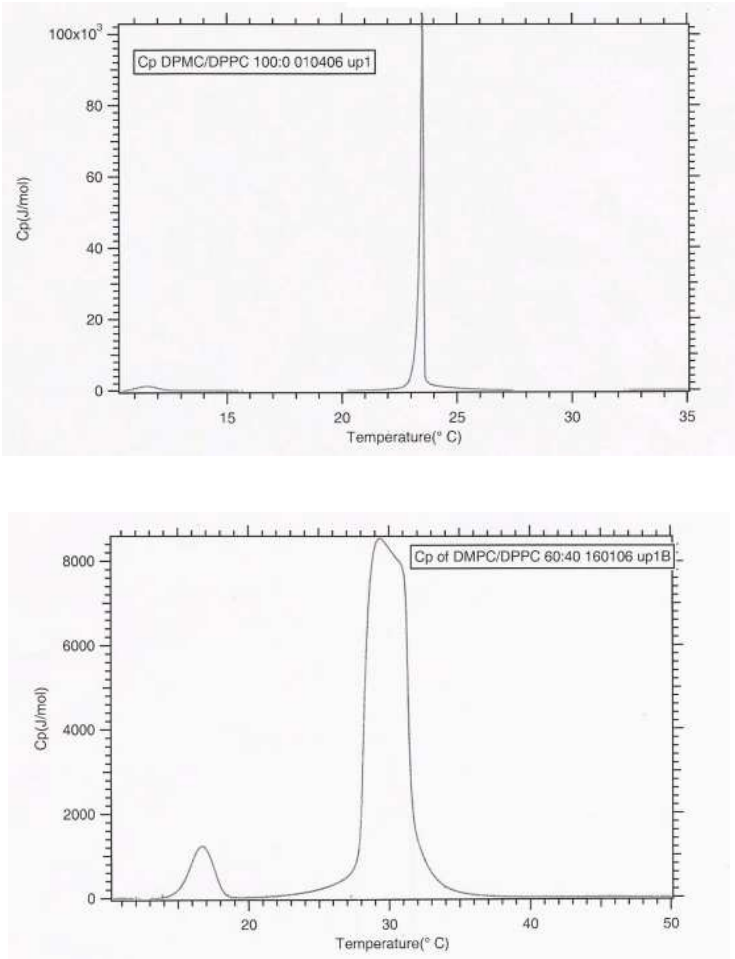

Figure 4: Heat capacity curves for pure DMPC (above) and a DMPC/DPPC 60:40 lipid mixture (below).

There are many results indicating that the organization of lipid membranes is not random. There is evidence of a lateral small-scale structure in bilayers (and monolayers) in the nanometer and micrometer range, both in biological and model membranes. These so called domains (or rafts) are often dynamic. Lipid bilayer fluctuations are either local density variations or variations in molecular

composition. Domain formation do not only appear in lipid mixtures, but can also occur in one-component lipid bilayers. Simulations show that the bigger the disparity in chain length, the bigger the domains.[5] There is both indirect and direct evidence of domain formation. One indirect way is to use fluorescence resonance energy transfer (FRET). By using a donor and an acceptor that have a propensity towards different phases, we can by looking at the measured fluorescence intensity detect the phase transition. An increase in fluorescence from the donor is explained by a larger distance between donor and acceptor, thus implying phase separation. This technique is sensitive to domain formation on the order of 10 nm.[9] As direct evidence we have different imaging techniques such as fluorescence microscopy and atomic force microscopy (AFM) [5]. Figure 5 shows fluorescence images of domains taken with a confocal microscope.

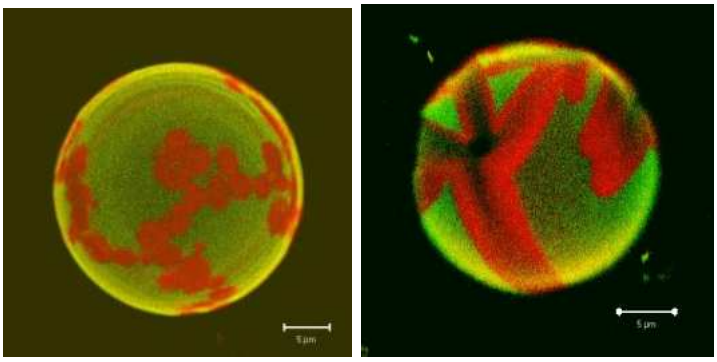

Figure 5: Confocal images of GUVs. Left: DLPC/DPPC 30:70. Right: DMPC/DPPC 50:50.

Domains in biological membranes are often smaller and harder to see by direct imaging, but there are several experiments done suggesting the existence of these domains often referred to as rafts. Experiments show that proteins can be temporarily confined to a region of the membrane, diffuse around and then jump to another region. These rafts contain a lot of cholesterol and shingolipids. Cholesterol has a tendency to stiffen membranes and induce a liquid-ordered phase when present in model phospholipid membranes. This phase corresponds to positional disorder combined with a high degree of conformational order. There is only limited evidence that this would be the case in the raft like domains present in biological membranes, but it is clearly an interesting thought.[5] These rafts are often seen as rather static, but computer simulations suggest that it would be likely for them to be subject to large fluctuations [10]. But the whole raft versus domain discussion is quite confusing and it is hard to clearly define what is meant by the one and the other. There are some indications that the lipids alone control the domain formation and that proteins are not needed for that process [5].

What role does these domains play in the functionality of membranes? What is their effect on permeability, binding affinity, bending rigidity and so on? In this master thesis we will concentrate on investigating how domain formation in

the phase transition regime affects the elasticity of model DMPC/DPPC giant unilamellar vesicles.

1.2 What to study and why?

Using electroformation we made giant unilamellar vesicles that we studied by means of optical tweezers (OT). This was complemented by calorimetric studies of the used lipid mixtures as well as confocal fluorescence imaging of vesicles. These techniques will be explained in more detail further on. We deformed lipid vesicles by tightly focusing a 1064 nm laser beam inside them. Both temperature and laser power were varied. For each temperature the laser power was gradually risen from 0mW to a maximum of 575mW. Here follows an image series of a GUV deformed at two different temperatures. Already from this we can suspect a temperature dependence of the observed deformations.

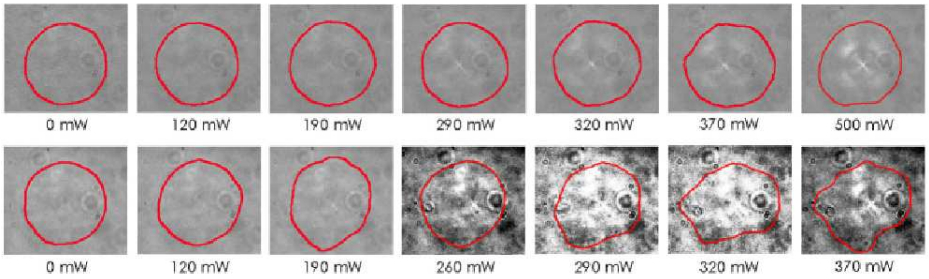

Figure 6: Brightfield image series of laser-induced deformations. Above: T=22°C. Below: T=33° C. The same vesicle was used at both temperatures. The red lines help visualizing the contour of the vesicle.

Why is the observation and quantification of direct deformation of membranes by optical tweezers interesting? Since many OT studies are made on living cells, it is relevant to try to understand the effects of light on membranes. Infrared or near-infrared lasers are often used for trapping biological cells since they are thought to affect them only marginally [8]. Although biological membranes are quite different and much more complex, it is still relevant to study how model membranes are affected.

We can also extract information about the membrane elasticity by trapping a GUV in optical tweezers. How much a vesicle deforms is highly dependent on phase and hence can be controlled by varying the temperature. By probing this dependence with means of OT, we could then compare the critical laser powers at which a different deformation regime occurred with heat capacity profiles measured by differential scanning calorimetry. The phase dependent elastic behavior of lipid membranes might be highly relevant for biological functions since the phase transition can be shifted by many different environmental factors such as pH, pressure or temperature.

2 Materials and methods

2.1 Differential Scanning Calorimetry

2.1.1 Method

Differential Scanning Calorimetry (DSC) is a powerful tool for the study of endothermic and exothermic processes like chain-melting phase transitions in membrane systems, both biological and artificial [17]. DSC is also the most direct method to access the thermodynamical mechanisms behind conformational changes of biological macromolecules. For instance the method is useful for the study of binding processes like the interactions between macromolecules (intermolecular recognition), protein folding and stability (intramolecular recognition) or a combination of both. In those cases DSC is often combined with isothermal titration calorimetry. To know more see [18], [19] and [20]. We will now focus on the study of lipid phase transitions by means of DSC. Small molecular weight molecules like lipids cannot be examined by DSC unless they form aggregate structures [20]. Fortunately lipids membranes are highly cooperative.

A differential scanning calorimeter has two cells that are adiabatically isolated. One is filled with the reference and the other with the sample solution. The temperature is changed at a constant rate and the temperature difference between the two cells is maintained at zero [22]. If a process takes place in the sample but does not occur in the reference, different powers are needed to heat or cool the two cells.[21]

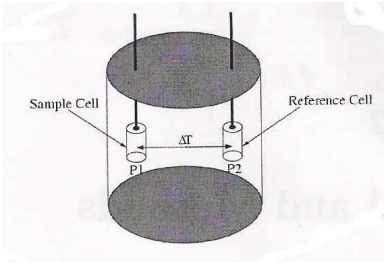

Figure 7: Schematic drawing of a differential scanning calorimeter [17].

For a detailed diagram of a VP calorimeter see figure 14.1 in [20].

The heat difference ΔQ is proportional to the power difference ΔP:

$$\Delta Q = \int_{t}^{t+\Delta t} \Delta P dt \simeq \Delta P \Delta t \tag{2}$$

ΔQ is in turn proportional to the excess heat capacity ΔC_p by the following thermodynamical relation:

$$\Delta C_p = (\frac{\partial Q}{\partial T})_p \approx \frac{\Delta Q}{\Delta T} \approx \frac{\Delta P}{\frac{\Delta T}{\Delta t}} \tag{3}$$

Where $\frac{\Delta T}{\Delta t}$ is the scan rate [17].

If the thermal event that occurs is endothermic then more heat is needed and there is an upward deflection of the Cp-curve. If the process is exothermic the deflection is downward [22].

The enthalpy change ΔH can be obtained by integrating the Cp-curve since

$$\Delta C_p = (\frac{\partial H}{\partial T})_p \tag{4}$$

for a reversible process.

The enthalpy change can be used to calculate the bending modulus of a membrane at the main phase transition.

We can also get the change in entropy associated with the transition [22]. At the melting point the change in Gibbs free energy $\Delta G = 0$ [23].

$$\Delta G = \Delta H - T \cdot \Delta S \tag{5}$$

This gives:

$$\Delta S = \frac{\Delta H}{T_m} \tag{6}$$

2.1.2 Sample preparation

For the calorimetry experiments 10 mM stock solutions of DMPC and DPPC were prepared. The lipid powder (Avanti Polar Lipids, Alabaster, AL, USA) was dissolved into 4 ml of organic solvent; a mixture of Dichloromethane/Methanol in a volume ratio of 2:1. From these stock solutions we could then prepare samples in the desired molar ratios ranging from 100:0 to 0:100 in 10-steps. The samples were dried by being heated under a very light air stream to help the evaporation of the last of the solvent. The dried samples were put in a desiccator overnight and then kept in the freezer.

Before making the calorimetry scans the samples were rehydrated with the same volume of millipore water (with a resistance of 18MΩ) as organic solvent before

evaporation. During this process they were heated up to 60 °C and stirred with a magnet for one hour. Every 10-15 min the sample was vortexed in order to help the lipids to detach from the inside of the glass vial and make the sample more homogeneous. During rehydration small multilamellar vesicles form in the lipid suspension [22]. Before put into the calorimeter the sample and the reference, in our case millipore water, were stirred with a magnet in a vacuum pump in order to remove air bubbles that could have disturbed the measurements.

2.1.3 The experiment

To make the heat capacity measurements a VP differential scanning calorimeter from MicroCal (Northhampton, MA, USA) was used. First the millipore water was put into the right cell of the calorimeter with help of a glass syringe. The cells can hold 0,5152 ml each. The excess liquid was then carefully removed. The edge of the cell was easily found by slightly bending the needle when taking it out. The same was done in the left cell with the lipid sample. The excess sample was put back in the vial for a possible later use.

Figure 8: The used VP differential scanning calorimeter.

VP-Viewer was used to control the scan parameters. Two up scans were made at a scan rate of 5 °C/hour as well as two down scans for control. The starting temperature was set to 10 °C and the final temperature to 50 °C. The filtering period was set to 10 seconds, this being the time interval during which calorimetric data is collected and averaged. We chose a high feedback so that the calorimeter would react fast to changes in the system, the trade-off being a lower sensitivity. Before starting every scan the pressure was set to 50 psi.

2.2 Confocal Microscopy

2.2.1 Method

The confocal microscope (CM) combined with fluorescent labeling of the sample has become a powerful tool not only for 3D imaging of sample structure, but also for the imaging and understanding of cell function. Though the concept of confocal microscopy was patented in the late fifties, it really became popular once progress in computer technology made it easy to store and work with digital images.[24] The confocal laser-scanning microscope (CLSM) was commercially available in 1987 [27].

In widefield microscopy the whole sample is illuminated. The emitted light from areas above and below the focal plane of the objective lens contribute to out-of-focus blur. This reduces contrast and resolution and makes it harder to detect small structures in the sample. In confocal microscopy almost all the out-of-focus light has been eliminated. The illumination of the sample is sequential. The light is focused onto a very small spot that scans the sample in a raster pattern. This already reduces the illumination of the areas out of focus and hence reduces the blur. But the major feature of the CM is a spatial filter, a pinhole, that only lets through the light coming from the focal plane (see figure 9).[24][29] A barrier filter can also be used before the pinhole so that only wanted wavelengths are let through. For typical confocal images see [28].

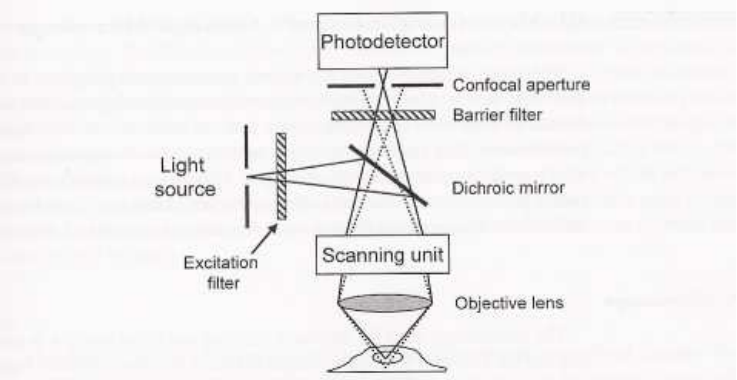

Figure 9: Basic design of a confocal microscope for use in fluorescence microscopy [24].

The size of the focal spot and thus the resolution of confocal as well as widefield microscopy depends on the wavelength of the illuminating light and the numerical apertures (NA) of the objective and condenser. The NA of a lens depends in return on the half-angle α of the cone of light acceptable by or emerging from it and the refractive index (n) of the medium between the lens and the sample [27].

$$NA = n \sin \alpha \tag{7}$$

For example, if α is increased the focal spot size decreases [30]. We can distinguish between lateral (parallel to the focal plane) and axial (along the optical axis of the microscope) resolution. For confocal microscopy, lateral resolutions between 140nm and 250nm and axial resolutions between 500nm and 1μm have been reported [24][29][30]. The image in focus of an infinitely small luminous point is not infinitely small, but is a circular Airy diffraction image with a central bright disk and dimer concentric dark and bright rings. The radius of the disk is:

$$r_{Airy} = 0.61 \frac{\lambda_o}{NA_{obj}} \tag{8}$$

where λ_o is the wavelength of light in vacuum and NA_{obj} is the numerical aperture of the objective. So two equally bright spots are resolved and seen as two if the distance d between them is equal to or greater than r_{Airy}. This is known as the Rayleigh criterion.[27] Also the size of the pinhole matters. Theoretically, the pinhole should be of the size of the Airy disk in order to increase axial resolution. This is accompanied though by a decrease in image brightness that might be a problem when studying dim specimens.[24] The ultimate limit of resolution (spacing at which the image contrast of periodically spaced objects drops to zero) obtainable with coherent confocal microscopy has been found to be identical to the one obtainable with incoherent non-confocal microscopy. However, as the spacing period is increased contrast rises much more sharply with coherent confocal microscopy, so the practical resolution is expected to be greater with confocal optics.[27]

The big advantage of CM as said is that only in-focus light reaches the detector which increases contrast and detection sensitivity. It also allows to section a sample without physically slicing it. Since optical sectioning is relatively noninvasive it makes it easier to study living samples. Imaging in the xy-plane is of course possible, but also xz- and yz-sections can be made by taking one raster line from each xy-image in the z-stack. Since the optical sections are obtained in a digital format it is easy to process the data and for example make 3D projections of the specimen.[24]

CLSM still has a few limitations. There is a limited range of wavelengths available for fluorescent excitation. In conventional fluorescence light microscopy mercury lamps are often used that can provide a wide range of wavelengths using different filters [24]. There are also photobleaching issues and one should be careful not to overexpose the sample to the laser light. Some laser can't be used at their full power since it would damage biological samples. Sometimes autofluorescence of biological samples can be a problem.[29]

We will now look at some factors affecting the quality of confocal imaging. A difference in the refractive index between the sample and the objective immer-

sion media can cause the focal plane to move more or less than the microscope stage. This affects the resolution, especially the axial.[26][29] The choice of lens is important. For example the higher the NA of the objective lens, the thinner the slice that can be "cut". This applies close to the coverslip. Spherical aberrations should also be taken into account. If different dyes are used it is difficult to compare the measured fluorescent intensities since the sensitivity of photomultiplier tubes isn't the same for all wavelengths. The used spatial sampling distance is also important. It should at least be half the size of the smallest input feature.[26]

There are different types of confocal microscopes. In our experiments we used a slow-scan beam scanning confocal microscope. A beam scanning CM uses rapidly scanning mirrors on a stationary specimen. They are often used to study fluorescently labelled biological samples. It should be pointed out that slow-scan CLSM can't be used to investigate rapid processes since it takes approximately half a minute to get a complete image stack. For this a video-rate CLSM can be used. They are able to capture processes that take place in the millisecond range. There are also stage scanning confocal microscopes in which only the sample is moved. All confocal microscopes do not use coherent laser light. Spinning disk confocal microscopes use white light from a mercury lamp.[25] Other methods can also be used to make fluorescence imaging. Multiphoton excitation microscopy gives the advantage of no out-of-focus photobleaching and photodamage. An alternative way of removing out-of-focus light is to use widefield microscopy and then deconvolve the obtained images. Deconvolution can be used to improve CM images as well. For a comparison of the two methods see chapter 23 in [27].

2.2.2 Sample preparation

The sample preparation was almost the same for the confocal microscopy and optical tweezers (OT) experiments. 1mg/ml lipid stock solutions of DMPC and DPPC were prepared with chloroform as organic solvent. Also the lipidlike fluorescent markers DiI-C18 (1,1'-dioctadecyl-3,3,3',3'-tetramethylindocarbocyanine perchlorate)(DiI) and Bodipy (2-(4,4-difluoro-5,7-dimethyl-4-bora-3a,4a-diaza-s-indacene-3-pentanoyl) -1-hexadecanoyl-sn-glycero-3-phosphocholine) from Invitrogen were used. The DMPC and DPPC stock solutions were mixed in the desired molar ratios. DiI was added at a concentration of 0.125×10^{3}mol/L in the molar ratio DiI:lipids 1:500. Bodipy was added to the samples at a concentration of 0.113×10^{3}mol/L in the molar ratio Bodipy:lipids 1:250. The solvent was then evaporated by heating under a gentle nitrogen stream. When dried Trifluoroethanol (TFE) was added to the samples in the same amount as the chloroform present before evaporation (200μl). The samples were stored in the freezer. When preparing for experiments, 6μl of the desired sample was put on an Indium Tin Oxide coated 0.17 mm thick Borosilicate Thin Glass coverslip (ITO). The prepared ITOs where put in a desiccator overnight to remove all solvent residues.

2.2.3 Electroformation

The vesicle formation was done in the chambers used for confocal imaging respectively optical tweezers experiments. Even if the two chambers presented some differences the major features stayed the same. Two ITOs were separated by a 3 mm respectively 300μm thick spacer made of peek (a very robust plastic that can hold up to 160 °C before distorting), mounted on a metal sample holder through which water could be flushed, see figure 10. The sample holder was coupled to a heat bath, brought up to 60 °C and thereby heated the sample to a temperature above the phase transition. The electrical connection between the bottom ITO and its corresponding electrode was verified. The lipid film on the bottom ITO was rehydrated with preheated Millipore water with a minimum resistance of 18MΩ. Vacuum grease was used to make the ITOs stick to the spacer. A small hole, sealed with vacuum grease was made in the top ITO (1 mm thick) in order to monitor the temperature with a thermocoupler in the OT experiments. After approximately 20 to 40 minutes of hydration in the dark, to avoid photobleaching of the dyes, the spacer was electrically connected to a function generator supplying 10Hz, 2V sinusoidal alternative current. The duration of the electroformation was also of about 20 to 40 min. We got mostly semi-spherical vesicles attached to the bottom ITO, but in some cases the lipids formed detached spherical vesicles, especially if the current was left on for a longer time. The sample was finally cooled down on a well conducting surface before put into the microscope. Having the vesicles attached to the surface of the bottom ITO was an advantage in our case, making it possible for us to use the same vesicle throughout a measurement series.

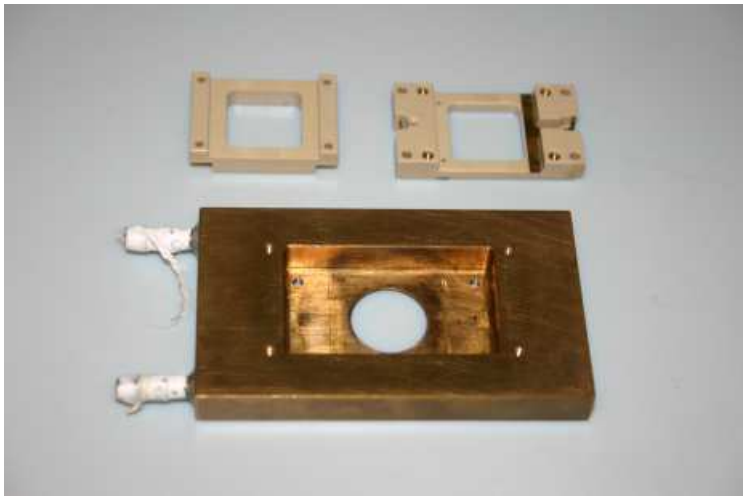

Figure 10: Sample holder for electroformation and confocal microscopy.

The mechanisms of vesicle formation are not well known. Experiments have been made were the sample was observed during vesicle formation [12][15]. The strength of the electric field and the thickness of the dried lipid film are two of the critical parameters for vesicle electroformation. The thinner the lipid film is

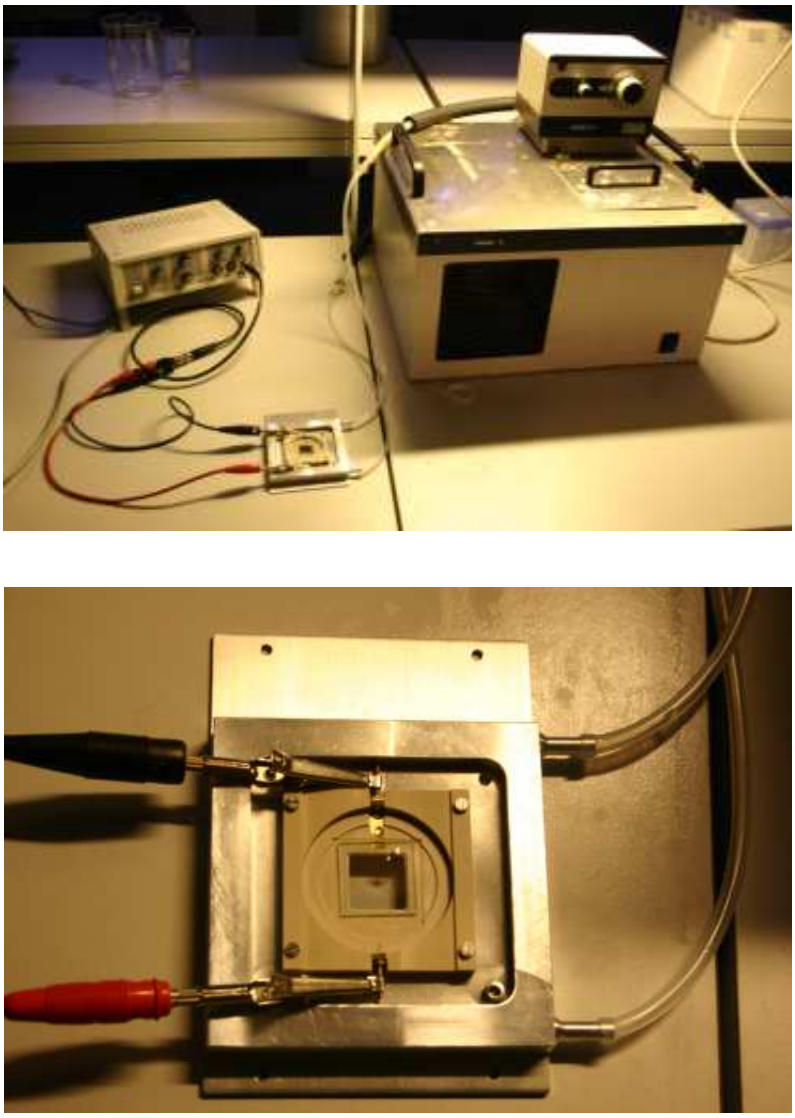

Figure 11: Electroformation: Above) Sample holder, function generator and heat bath. Below) Close up on the chamber.

the higher the yield of unilamellar vesicles. Swelling occurs almost immediately after the application of an electric field onto the sample. According to Angelova et al. [12] structures with a circular contour grow to a size of approximately 10μm after which a fusion process starts. Vesicles fuse together and grow to be tens of μm in diameter and finally detach letting new vesicles grow out of the lipid film. This was also observed by Mathivet et al. [15]. After approximately one hour the sample stays more or less the same.

So what drives the vesicles to form? Observations were made of a vibrating motion of all the vesicles in a sample matching the frequency of the applied electric field. This could be controlled by varying the intensity and the frequency of the field. This mechanical agitation must at least be one of the mechanisms of vesicle electroformation.[12] The formation of GUVs requires lipid layer separation and bending. The AC field has been shown to have a strong effect on the normal forces that cause repulsion between the lipid layers. Worth mentioning is also the possible effects of the AC field on lipid layer topology, for example pore formation that could favour the hydration of the lipid film and thus the vesicle formation.[14]

Other methods can be used to form GUVs, for example electroformation using Pt wire electrodes [16]. Also the gentle hydration and the solvent evaporation methods are used. There is no consensus on the conditions necessary to obtain GUVs but there are two important conditions: that the temperature during vesicle formation should be above the melting temperature of the used lipid mixture and that the sample shouldn't be agitated during vesicle formation [14]. The pro and cons of these different methods have been investigated in [13] and [14]. Electroformation seems to give rise to a higher yield of non-defect unilamellar vesicles with a more homogeneous size distribution (mostly between 10 and 30μm in diameter) compared to the gentle hydration method. But in return the latter can be used for making GUVs containing a quite high percentage of charged lipids, which is much more difficult using electroformation [13].

In fig.12 we can see some fluorescence microscopy images of vesicles. They show examples of the defects classified and quantified by Rodriguez et al. [13]. They define a defect as a lipid structures that makes a GUV differ from a unilamellar vesicle. Three types of defects are described. First, a "nest of vesicles" where one or more vesicles are enclosed in each other like Russian dolls. The second type is smaller vesicles or lipids aggregates inside a large vesicle. And the third is the presence of tethers connected to the inside or the outside of the membrane. For more details on the distribution of this defects depending on the used vesicle formation method, see [13]. Bleaching experiments were carried out by Mathivet et al.. Fluorescent long-chained phospholipids were added to the lipid mixture and a portion of the sample was then bleached. The bleached vesicles recovered their fluorescence after a couple of minutes. This suggests a connectivity between vesicles during the swelling period. One hypothesis is the existence of tethers, but they could not be directly observed.[15] Using two-photon excitation microscopy Bagatolli et al. were able to observe the coexistence of stable tethers or tubes with lipid vesicles. They found a heterogeneity in the shell thickness of these structures suggesting the existence of both unilamellar and multilamellar tubes.[14] The fluorescence intensity is proportional to the number of fluorescently labeled bilayers, so the use of fluorescence microscopy makes it possible to distinguish between multi- and unilamellar vesicles [13][14]. This can be of great help.

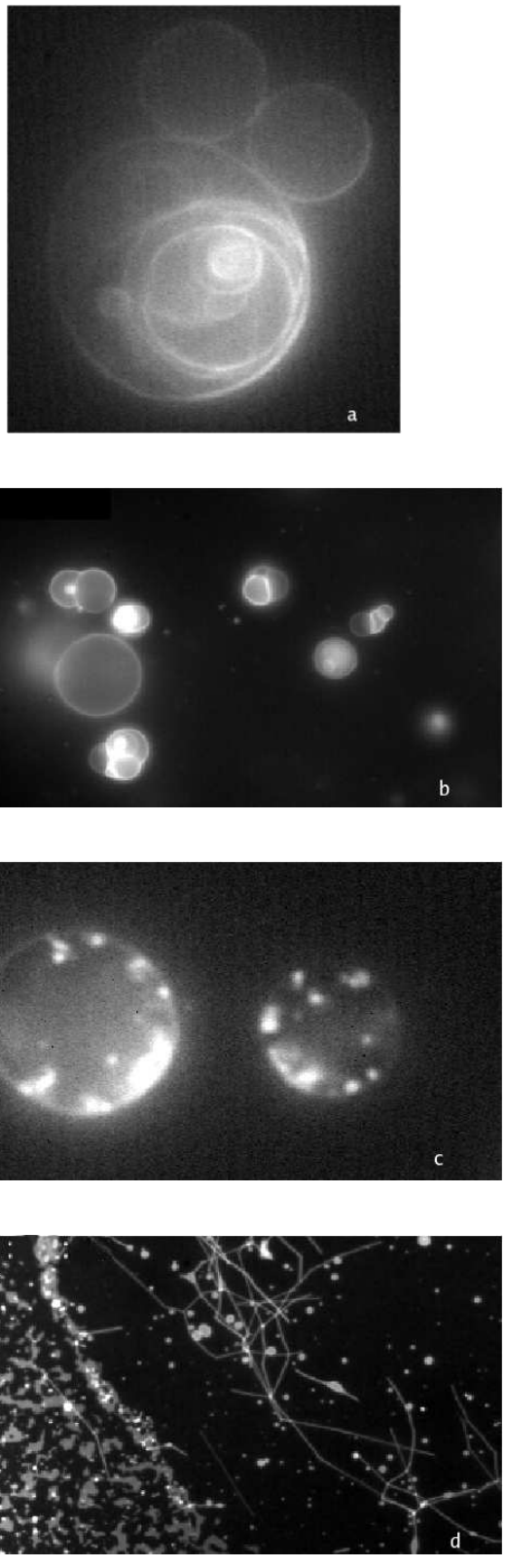

Figure 12: a)Nested vesicles, b) One unilamellar vesicles and vesicle aggregates, c) Lipid aggregates inside vesicles, d)Tube like structures.

2.2.4 The experiment

We wanted to visualize domains on the surface of GUVs. We looked at different lipid mixtures at different molar ratios: DLPC/DPPC 30:70 (DLPC: 1,2-Dilauroyl-sn-Glycero-3-Phosphocholine (12:0)) from Avanti Polar Lipids), DMPC/DPPC 50:50 and 70:30.

We used the microscope (Zeiss -LSM 510 META NLO, Carl Zeiss, Jena, Germany) in the fluorescence mode, using a HeNe laser, to excite DiI at 543 nm in order to see the vesicles and find an appropriate one to work with. Then we put on the Argon laser in order to excite Bodipy as well at a wavelength of 488 nm. We switched to the confocal mode. The pinhole was set to 80μm in diameter, the z-stack interval was 0.5μm and the scan speed quite high. We obtained a stack of images for every scanned vesicle (See Data and error analysis). The used objectives were either water immersion objectives with a NA of 1.2 or an air objective with a NA of 0.75.

We also made some heat experiments on DMPC/DPPC 50:50 vesicles to visualize the different phases of the lipid mixture. We started at 29 °C, then cooled down to 20 °C, heated up to 40.6 °C and finally cooled down to 30 °C again. In the binary mixtures we used, Bodipy prefers the fluid phase and DiI prefers the gel phase [31]. By choosing different colors for the Bodipy and the DiI signal channels we could visualize domains on the surface of the studied vesicles.

2.3 Optical Tweezers

2.3.1 Method and experimental setup

With optical tweezers it is possible to measure forces in the picoNewton range. This makes them a perfect method for studying weak interactions such as the motion of single proteins in a plasma membrane [36][37] and the stretching of DNA [33]. We will first go through the principals of optical trapping. A dielectric particle near the focus of a tightly focused laser beam will experience a force. This force has traditionally been divided into two components, a scattering force and a gradient force. There is a net momentum transfer from the incident photons to the particle near the trap. If the scatter is isotropic, as for a sphere, only the force in the direction of propagation of the light subsists.[35] When light passes through a for the light transparent object fluctuating electric dipoles are induced [34]. The interaction of these dipoles with the inhomogeneous electric field at the focus gives rise to the gradient force [35]. This force is proportional to the spatial gradient in light intensity and acts in the direction of the gradient [34]. It is also proportional to the polarizability of the trapped dielectric. For stable trapping a very steep gradient is needed, hence the necessity to sharply focus the laser beam using an objective with high numerical aperture. With a steep gradient in light intensity the axial component of the gradient force overcomes the net scattering force pushing the particle away from the focus of the trap. This balance between the two forces results in an equilibrium position

slightly beyond the focal point. The optical trap can be seen as a Hookean spring with a stiffness proportional to the light intensity.[35]

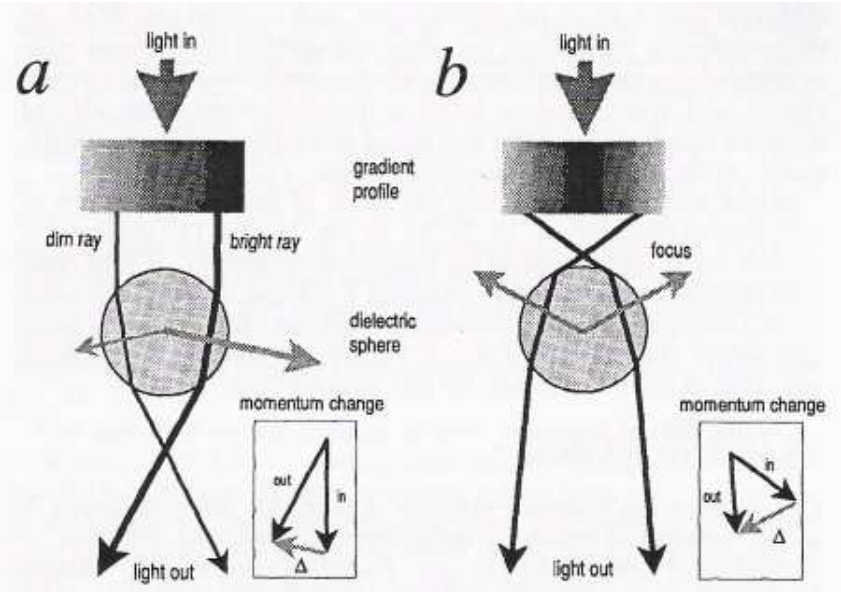

Figure 13: A ray-optic picture of the gradient force corresponding to the Mie regime. The dark gray arrows correspond the representative rays and the lighter rays correspond to the reaction forces. a) A parallel beam of light with a gradient in intensity shines through a transparent sphere with a higher refractive index than its background. The inset shows the change in momentum for the right ray. b) A single beam trap where the light is brought to a focus. This pulls the bead upwards. The inset shows the change in momentum for the left ray. [34]

Particles with sizes varying from several nanometers up to tens of micrometers can be trapped [34]. There are two limiting cases for which the forces on a sphere can be readily calculate. If the trapped particle is much larger than the wavelength of the trapping laser (the radius $a \gg \lambda$) the Mie regime is satisfied and simple ray optics apply. Refraction of the incident light corresponds to a change in momentum. According to Newton's third law an equal and opposite momentum change is imparted to the particle. The rate of change in moment gives the force acting on the sphere and is proportional to the light intensity. When the index of refraction of the particle is greater than the one of the surrounding medium the force is in the direction of the intensity gradient. Inversely if the refraction index of the particle is smaller than the one of the medium the force is in the opposite direction of the intensity gradient. In the Rayleigh regime the dimensions of the trapped particle are much smaller than the wavelength of the trapping laser ($a \ll \lambda$). In this case the light cannot be represented by rays, but trapping still occurs. Since in this limit the electromagnetic field is uniform across the trapped dielectric particle it can be treated as a point dipole and the scattering and gradient components can be readily separated. The scattering force is due to absorption and reradiation of light by the dipole. The gradient

force is still proportional to the intensity gradient. Unfortunately most biological work falls into the intermediate regime when the size of the trapped object is comparable to λ.[35][34]

The simplest and most straight forward implementation of optical tweezers is the manipulation of dielectric objects, such as micrometer-sized polystyrene beads [33]. These beads are good to work with since they are symmetric and also easily coated with diverse molecules. This makes them useful as handles to manipulate objects that are either very small or aren't easy to trap. The fact that they are spherical also makes it possible to do a precise position and force calibration [35].

One way of making lateral force calibration of an optical trap is to use the escape method by applying a drag force on the trapped particle. It is gradually increased until the particle escapes. This is done by moving the sample relatively to the trapped particle at a known velocity using a piezo stage. For small velocities the drag force F is proportional to the velocity v:

$$F = \gamma v \tag{9}$$

The drag coefficient γ is given by Stokes' Law:

$$\gamma = 6\pi\eta r \tag{10}$$

where η is the viscosity of the medium and r is the radius of the trapped spherical object. This gives the maximum force the trap can exert. The uncertainty of this method is of 20% approximately. For smaller forces a more precise calibration method using the thermal motion of a trapped bead can be used. In the plane perpendicular to the beam it feels an approximately harmonic potential near the focus due to the Gaussian shape of the intensity profile.

$$U(x) = \frac{1}{2}\kappa_x x^2 \tag{11}$$

where x is the lateral position of the bead and κ_x is the lateral spring constant of the trap, i.e. the trap stiffness. The Boltzmann distribution of position in a harmonic potential is:

$$p(x) \propto exp(-x^2/2\sigma_x^2) \tag{12}$$

By fitting this expression to a histogram of positions it is possible to determine σ_x. The equipartition theorem yields:

$$\sigma_x^2 =< x^2 >= k_B T/\kappa_x \tag{13}$$

This gives a value for the trap stiffness κ_x. There is an independent way of getting the trap stiffness. The motion of the bead in the trap is described by the Langevin equation:

$$F(t) - \kappa_x x - \gamma \dot{x} \tag{14}$$

where F(t) represents the thermal forces and γ is the drag coefficient. From that the following power spectrum is obtained:

$$S_x(f) = \frac{k_b T}{\pi^2 \gamma ({f_c}^2 + f^2)} \tag{15}$$

where $f_c = \kappa_x / 2\pi\gamma$ is the corner frequency. By fitting this expression to the data f_c can be found which then gives the trap stiffness. All this also yields in the y-direction. Comparing the values of κ_x (or σ_x) obtained by the two latter calibration methods provides a method for calibrating the response of the quadrant photodiode (in volts) to the position of the bead in the trap (in meters).[33][34][36]

The difference in refractive index between the immersion oil and the trapping medium leads to significant spherical aberrations. In practice, the use of an oil immersion objective limits the axial range of the trap to approximately 20 micrometers into the trapping chamber.[35] A water immersion objective can be used when it is necessary to trap deeper in the chamber. The trade off is that water immersion objectives often come with a lower NA and hence a less steep gradient and a bit weaker trapping force for the same laser power. The greatest light loss in OT lies in the objective. The output laser power isn't entirely transmitted through the objective [34]. For a Leica oil immersion objective as we used, the transmittance often lies between 50 and 60%.

Optical tweezers are well suited for working with biological samples, especially in the near infrared and infrared region (750-1200 nm) were there is a minimum in light absorption (see fig. 3 in [34]). This window of near transparency is due to a decrease in absorption by biological chromophores such as hemoglobin or proteins and water absorption is still quite low at those wavelengths [35][34]. One common laser frequency to work with is 1064 nm, which we also used in our experiments. The wave being continuous is also important. A pulsed laser would do greater damage, e.g. facilitate DNA denaturation [50]. The effect of near infrared lasers on model membranes and biological samples will be discussed further in the discussion chapter.

The optical tweezers setup was based on an inverted microscope. The laser used was a Nd:YVO_4 laser with a wavelength of 1064nm. Before entering the microscope the laser beam was walked through a series of lenses and mirrors. See figure 14. In the setup used for these experiments the telescope at the end of the path used one of the lenses inside the microscope. The back aperture of the microscope objective (100x/1.4 NA, oil, Leica) was overfilled with the laser beam

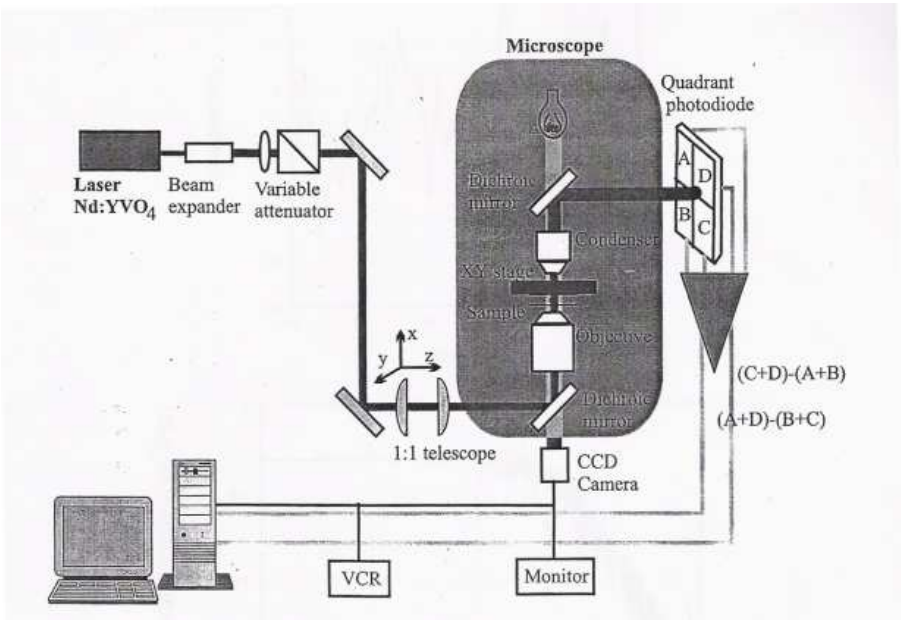

Figure 14: Schematic diagram of the optical tweezers setup [33].

to ensure that the light converged to a tight spot. The sample was illuminated from above. A CCD-camera was used for sample imaging. The trapping laser was also used for the position detection of the trapped object. After being focused on the sample by the objective the laser beam was collected by a condenser with high NA and projected on a quadrant photodiode by a dichroic mirror. A piezoelectric stage was mounted on a spring-load translational stage making it possible to control positioning with nm precision.[33] A mercury lamp was also mounted to the microscope in order to take fluorescence images of the sample.

2.3.2 Sample preparation

The sample preparation was the same as for the confocal microscopy experiments excepted for three things. Dichloromethane/Methanol in a volume ratio of 2:1 was used instead of chloroform, air was used instead nitrogen to dry the samples and only the dye DiI was used.

A new chamber was made for the OT experiments (see figure 11). It was derived from the one used for making confocal imaging, but the space between the two ITOs had to be made much smaller; 300μm to 500μm instead of a few millimetres. This would have been really important if accurate force measurements could have been carried out, but still it gave a better illumination of the sample and a better image quality. The vesicle preparation was otherwise identical to the one carried out for the confocal imaging experiments.

Figure 15: Optical tweezers setup.

2.3.3 The experiment

The outline of the experiment was to measure the temperature dependence of the deformation of GUVs by means of optical tweezers. For every chosen temperature a series of images were taken with stepwise increased laser power.

To be able to control the temperature inside the chamber, we heated (or cooled) the sample holder with the help of a heat bath. The oil objective needed to be temperature controlled as well since the immersion oil is a good heat conductor. For this purpose we used a self-designed objective heater connected to the sample holder as well as the heat bath by silicon hoses. In order to obtain the wished temperature inside the chamber, we made a calibration curve (see figure 16) to make it easier to find the proper heat bath settings. The temperature of the sample was still monitored by a thermocoupler during experiments. No compensation for the loss of heat through the condenser was made. Figure 16 shows the effect of that loss on the sample temperature.

Once the sample was put into the microscope, we used the laser at a power of approximately 750 mW to find the surface of the bottom ITO by looking for

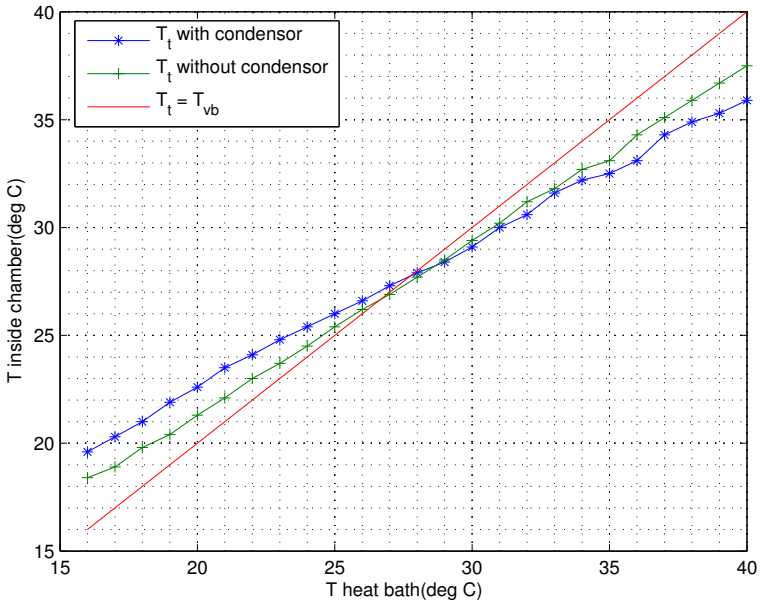

Figure 16: Calibration curves for temperature control of the chamber.

the reflected laser light on the glass surface. This was very helpful since the vesicles, assuming there were any, were almost transparent and therefore much harder to spot than for example a polystyrene bead. We did not calibrate the trap since the light was directly interacting with the lipid membrane. The laser power needed to trap a bead heavily deformed the vesicles and made any viable force measurement impossible. All laser powers mentioned in this report will be laser output powers and not the laser powers in the trapping region. The power in the trap is approximately 20% of the output power. The surface of the bottom ITO was set as the zero level (0 μm). Then we looked for vesicles with the help of fluorescence microscopy using a Leica Mercury-lamp with a TX2 (Texas red/green) filter cube having a BP 540-580nm excitation filter and a BP 608-682nm suppression filter. These filters approximately fit the emission and absorption spectra of DiI (see figure 17).

When a big vesicle was found, with a typical size varying between 15 and 30 μm and a nice round shape, the center of the trap was placed approximately one third up from the base of the semi-spherical vesicle. After setting the temperature and letting it stabilize we recorded with a VCR what was caught by the CCD-camera. Later, image series of vesicles deforming for stepwise increasing powers could be grabbed from the video tape. For every laser power a "10s off, 10s on, 10s off, 10s on, 10s off"-series was recorded. The laser power was controlled by increasing or decreasing the laser diode current in 0.1A-steps. A smaller step size would have been preferred, but could not be obtained. For small laser powers like the ones used in this experiment, the relation between

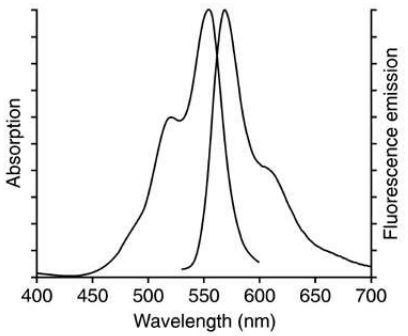

Figure 17: Absorption and fluorescence emission spectra of DiI bound to a phospholipid bilayer membranes[32].

diode current and output laser power was nearly linear.This resulted in a step size of approximately 35-40 mW. The laser power was increased until the studied vesicle reached a critical degree of deformation that threatened to make it burst. After what the temperature was reset and the same procedure was repeated. One vesicle rarely made it through more than two temperature series. The obtained images were then analysed to get a measure for the deformation of the vesicles.

3 Data and error analysis

3.1 Differential Scanning Calorimetry

An IgorPro program was used to analyze the heat capacity curves obtained from the DSC scans. In order to get only the signal from the lipids, the baseline was subtracted from the loaded heat capacity curve. This lacks a link to physical theory but in return is very easy to do and gives a good approximation of the enthalpy change [38]. The baseline fitting was done by fitting a polynomial function with degree varying between 3 and 5 to the heat capacity curve after removing the transition peaks. By integrating the area under the curve at the main phase transition we obtained a measure for ΔH, the change in the enthalpy of the system. The tangent method was used to determine the beginning and the end of the main phase transition in order to build a phase diagram of the DMPC/DPPC system. Also the melting temperature (T_m) was determined. In figure 18 we can see how this was done.

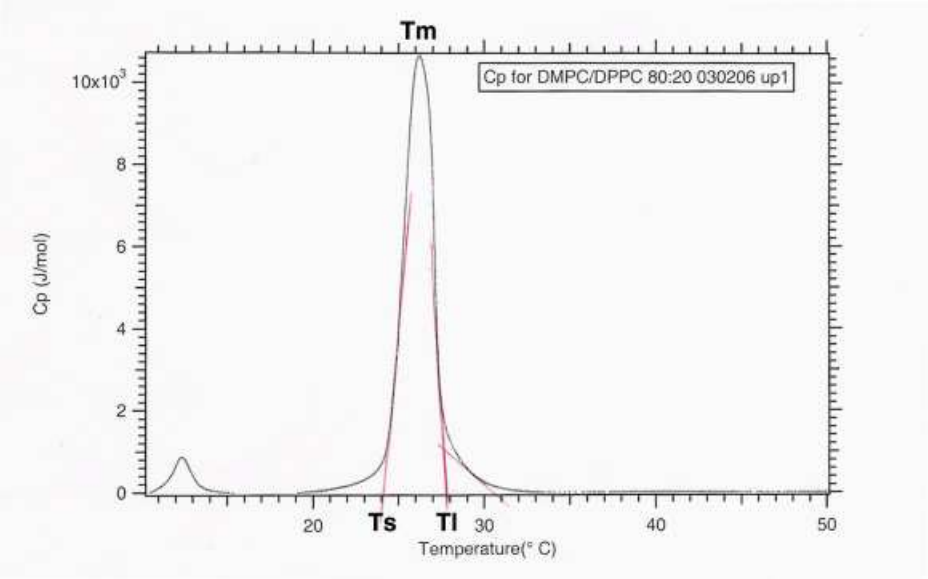

Figure 18: Determination of the phase boundaries for DMPC/DPPC 80:20 using the tangent method.

One of the sources of error we should be aware of is that of the baseline fitting. There isn't just one way of drawing the tangent and this affects both the end (T_l) and starting (T_s) points of the phase transition as well as the value of the enthalpy change. Though, as said before, the phase transition has no real sharp boundaries, so the uncertainty in the position of the end and starting points of the transition is not that bad.

The lipid powder was weighed on a scale with a precision of 1mg which made this step vulnerable to errors since we were weighing masses of a few milligrams. To minimize this source of error we made enough lipid stock solution to make several samples at the same time. Making several samples at the same time also showed to be time saving.

3.2 Confocal Microscopy

The LSM_FCS software the microscope was equipped with by Zeiss was used to control the confocal microscope and make the vesicle images. Part of the work on the confocal images was done while scanning the sample by correcting for the photobleaching of the dyes, especially Bodipy. Afterwards, a 2D- or 3D-projection of the image stack could be made and the contrast readjusted for each channel separately or together. Also the colors representing the signal from the different channels, hence the different dyes, could be chosen freely.

Sometimes the rim of the vesicle appeared brighter than the rest. This could be due to optical effects. Either the same amount of photons was emitted by the rim of the vesicle as from the top part, but ended up on a smaller area of the photodetector. It could also be that we started scanning a little below the equator of the vesicle and therefore got several pictures in the stack that all contributed to the same part of the 2D-projection, making the rim look brighter.

The temperature control of the experiment was not 100% accurate. Heating too fast induced a water flux inside the chamber from the inside out (maybe starting from the thermocoupler) causing the vesicles to migrate away from the center of the chamber.

3.3 Optical Tweezers

Having done our experiments we ended up with a lot of images of vesicles at different temperatures and laser powers. For every laser power ten pictures were saved to get meaningful error bars using the standard deviation of the data (the exceptions will be pointed out). The images were grabbed from the video tape using IMAQ Vision Builder and Measurements and Automation. As we will discuss in more detail in the results chapter, we wanted to calculate the ratio between the circumference and the area of a cross-section of the studied vesicles. The contrast between the contour of the vesicle and the background being too low it was very difficult to use Matlab's image toolbox directly. Therefore we marked the rim of the vesicle in every image "by hand" using the function *roifill*. This gave us a black and white (BW) image from which we could get the area of the vesicle cross-section by summing up the image-matrix. The function *edge* was then used on the BW image to get the circumference. The ratio circumference through area (C/A) was calculated for every picture. C/A was then plotted against laser power for every temperature and lipid composition (DMPC/DPPC 50:50 and 70:30).

We also wanted to know if there was a laser power at which we could observe a dramatic change in the deformation, i.e. in the ratio C/A. Determination of this critical power was made by fitting a fourth grade polynomial to the obtained data using matlab. Two tangents were then drawn. We defined their intersection as the critical power P_c.

One of the encountered problems was that one vesicle rarely survived more then two measurement series (measurements at two different temperatures). Even if they did not burst they went through some none reversible shape changes at the base that influenced the whole vesicle shape. Making measurements on different vesicles affected the starting points of the C/A curves, but should not have affected the overall behavior of the vesicles.

One source of error was the drift in the system during experiments. The zero level needed to be readjusted from time to time which means that a certain discrepancy may have occurred between the measured C/A ratio and the actual C/A ratio at the right height. This could have affected the smoothness of the plots.

A smaller step size and hence more data points (especially at higher laser powers) would also have helped getting smoother curves and made the determination of the critical power more accurate.The vesicles also got out of focus at high powers. This combined with strong shape fluctuations lead to large error bars since fewer images could be taken and the contour of the membrane got harder to determine.

One other thing that needs to be underlined is the fact that we analyzed the shape change of a cross-section of a vesicle and not the shape change of the whole GUV. We have for example no clue on the displacement of the top of the vesicle.

4 Results

4.1 Differential Scanning Calorimetry

The measured heat capacity profiles of the two studied mixtures are shown below.

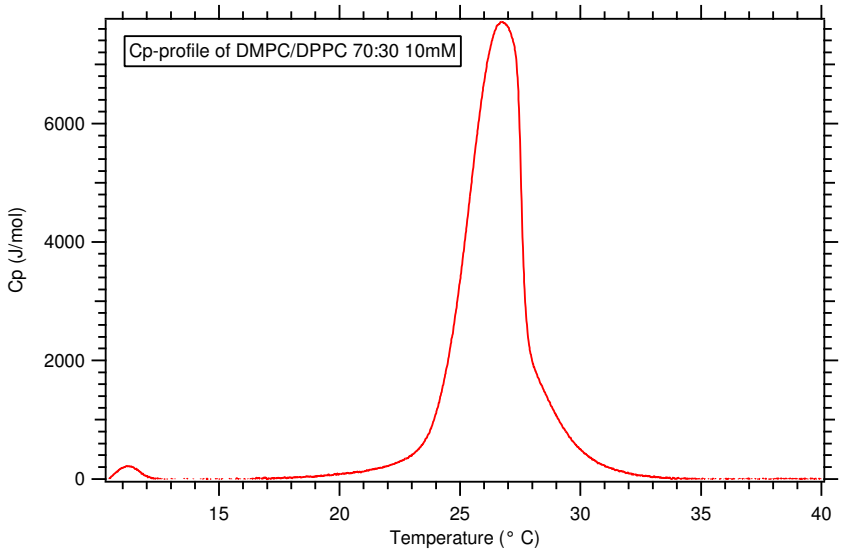

Figure 19: Heat capacity profile of a DMPC/DPPC 70:30 mixture.

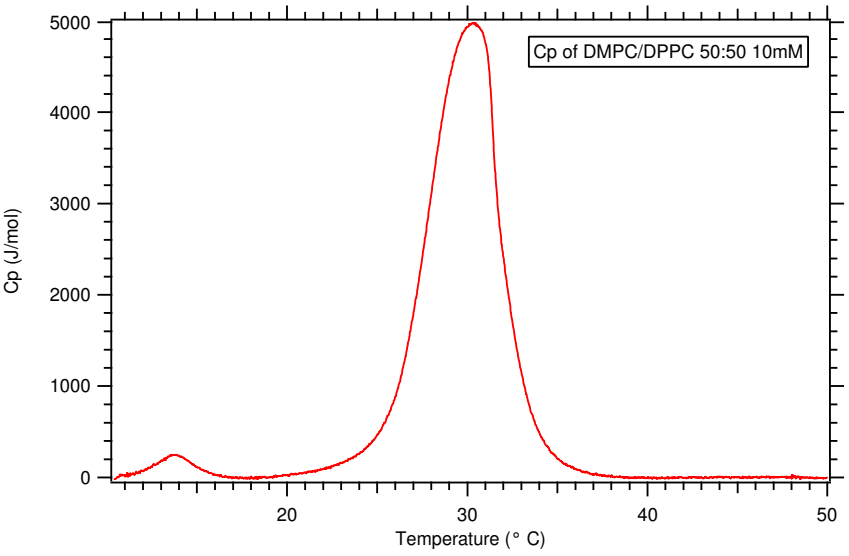

Figure 20: Heat capacity profile of a DMPC/DPPC 50:50 mixture.

The Cp-profiles of DMPC/DPPC mixtures only show one maximum. For lipid mixtures with greater chain length or structure disparities two merged peaks can be observed due to a big difference in melting temperature [41]. The transition peak is broader for DMPC/DPPC 50:50 than for 70:30 since the two components contribute as much to the phase transition process. T_m of 50:50 is a little bit closer to the T_m of a pure DMPC lipid solution. See table in this subsection.

Here follows a table with the start (T_s) and ending (T_l) temperatures of the phase transition, the melting temperature (Tm) and the transition enthalpy change (ΔH) for DMPC/DPPC 50:50 and 70:30, as well as T_m and ΔH for pure DMPC and DPPC lipid suspensions.

Lipid composition	$T_s(^\circ C)$	$T_l(^\circ C)$	$T_m(^\circ C)$	$\Delta H(J/mol)$
DMPC/DPPC 50:50	25	34	30.3	25 295
DMPC/DPPC 70:30	24	30	26.8	23 894
Pure DMPC	-	-	23.5	24 457
Pure DPPC	-	-	41	23 783

Since the transition peak is so narrow for pure DMPC and pure DPPC there is no real point in estimating T_s and T_l. The values for the enthalpy change can be used to estimate the bending modulus of the membrane [43], though this wasn't done in this thesis.

Cp-profiles of ratios ranging from 100:0 DMPC/DPPC to 0:100 DMPC/DPPC in 10-steps were also measured. From these profiles and using the tangent method (see section 3.1) we constructed a phase diagram of the binary mixture DMPC/DPPC (see figure 21).

The lower boundary of the phase diagram is not as well defined as the upper boundary. The tangent method is not an exact method to determine the boundaries of the phase transition, but there would be no sense in having a more accurate method since there is in practice no sharp boundary to the phase transition and where it starts and ends differs slightly from one scan to the other. Only in the ideal case there is a sharp and well defined limit [41]. Still it is relevant in the sense that it gives us a clue on where to look for phenomena related to the phase transition like the phase coexistence of the solid-ordered and liquid-disordered phase and the resulting domain formation. Even though it is possible to find domains outside the transition, domain formation is preponderant while the system is in the transition regime. Still there is a quite good coincidence with earlier constructed phase diagrams [39][40].

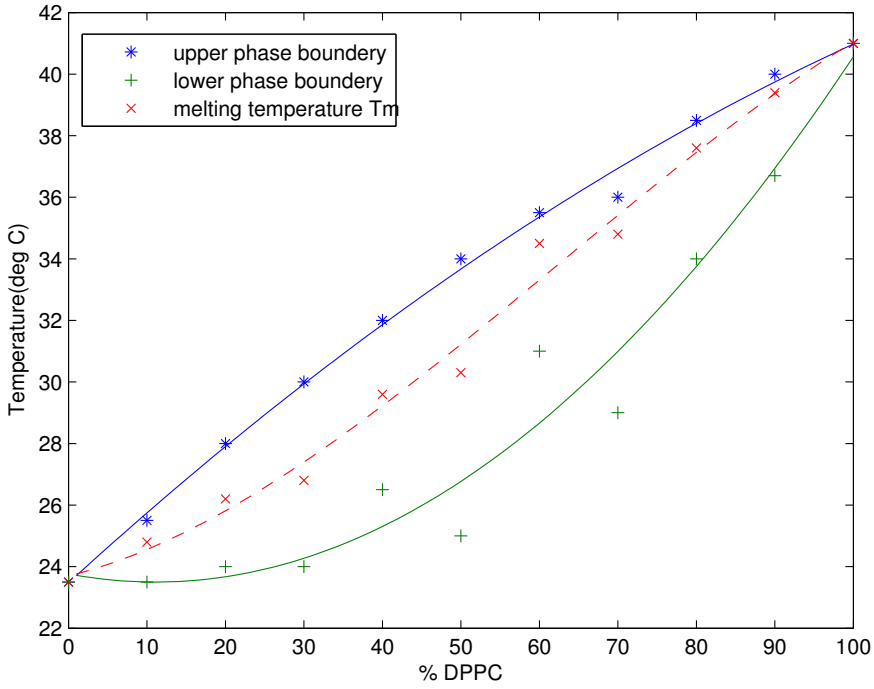

Figure 21: Phase diagram of the lipid binary mixture DMPC/DPPC.

4.2 Confocal Microscopy

So far we have a thermodynamical view of the phase transition. One more visual way is to use confocal fluorescence microscopy to observe the formation and structure of domains on the surface of vesicles.

One thing that can be investigated is the structure, i.e. the shape of the formed domains depending on lipid composition. We took images of DLPC/DPPC and DMPC/DPPC vesicles (See figure 22). The binary mixture of DLPC/DPPC seems to give rise to round domains with an approximate diameter of 2 μm connected to each other. On the other hand a DMPC/DPPC 50:50 mixture gives rise to more elongated and sharp domains, but interconnected as well. The broadness of these bands seems to vary between 0.5 and 5 μm (see also figure 23). This is just a hint of what can be observed on this subject. Others have done much more thorough studies on the influence of lipid composition on domain structure [42].

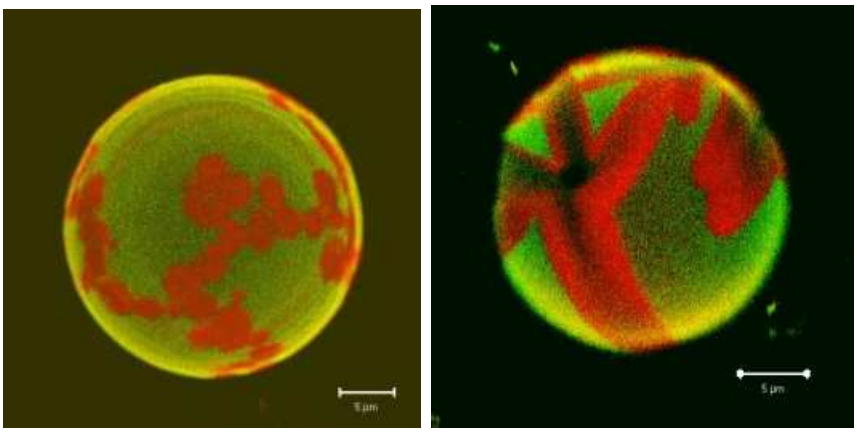

Figure 22: Left: DLPC/DPPC 30:70 vesicle at room temperature. Right: DMPC/DPPC 50:50 vesicle at T=29.9°C.

We also performed temperature dependence experiments and took pictures showing the different phases of the DMPC/DPPC 50:50 lipid binary mixture (see figure 23). We can clearly see a change in the repartition of the two dyes depending on temperature. Bodipy (green) has a greater affinity for the fluid (liquid-disordered) phase and DiI (red) for the gel (solid-ordered) phase. At temperatures T=26 °C and T=29.9 °C corresponding to the phase transition we can see that the two dyes are well separated and that domains are formed. The amount of DMPC in the green liquid domains is likely to be higher than the amount of DPPC and vice versa, since DMPC has a lower transition temperature T_m than DPPC. Above the transition, at T=40.6 °C the two dyes are quite homogeneously mixed and no signs of phase separation can be seen except maybe for a few small domains less than a micrometer big. Both DMPC and DPPC seem to be in the liquid-disordered phase. At T=22.9 °C, just at the lower boundary of the phase transition of the DMPC/DPPC mixture, a majority of the lipids should be in the solid-ordered phase, but there is a strong segregation of the two dyes and at least one domain is clearly visible. This could be an effect of rapid cooling, the DiI not having the time to mix with the other molecules before the membrane got more ordered and therefore stiffer, thus making diffusion processes slower.

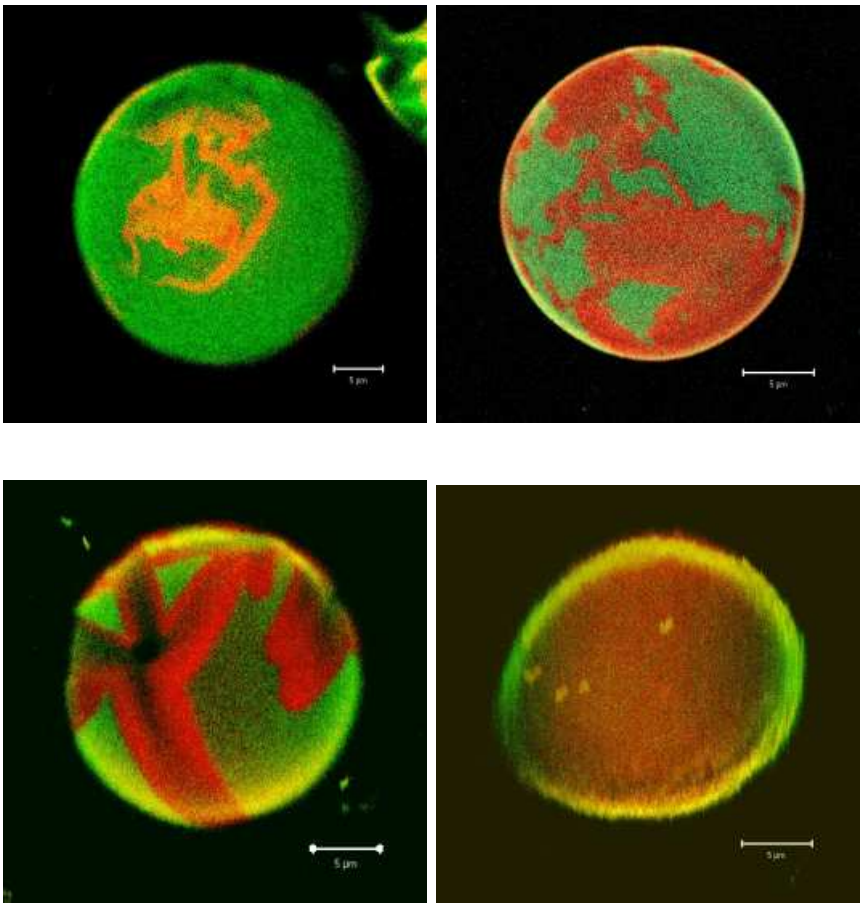

Figure 23: DMPC/DPPC 50:50 vesicles. Top left: T=22.9°C, top right: T=26°C, bottom left: T=29.9°C, bottom right: T=40.6°C.

4.3 Optical Tweezers

4.3.1 Observations

We have a thermodynamical description of the phase transition between solid-ordered and liquid-disordered states and a way of visualizing the resulting phase separation and domain formation. But what happens to the membrane's elastic properties when in the transition regime? We will start by looking at three typical brightfield image series of a vesicle deformed at constant temperatures T=22.4 °C, T =29.5 °C and T=33.5 °C and stepwise increasing laser power.

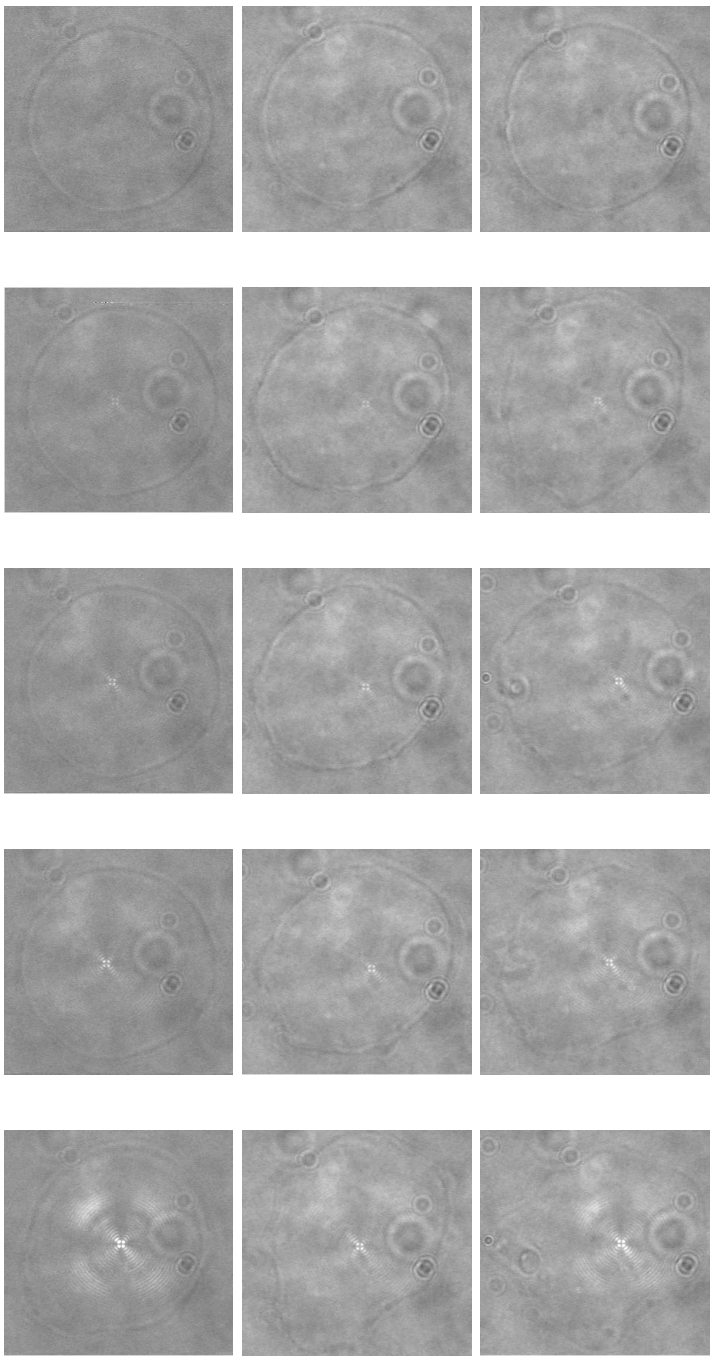

Figure 24: All three image series are of the same vesicle. Left: Series D, T=22,4°C, output laser power from top to bottom: 0mW, 190mW, 260mW, 293mW, 500mW. Middle: Series E, T=29,5°C. Right: Series F, T=33,5°C, output laser power from top to bottom, both for middle and right: 0mW, 190mW, 260mW, 293mW, 370mW.

At T=22.4 °C (Series D) the GUV is visibly less affected by the laser trap than at T= 29.5 °C (Series E) and T= 33.5 °C (Series F). With the laser power set to 293 mW the vesicle is still quite spherical, just starting to show signs of deformation. At 500mW (higher power than the vesicle could stand at T=29.5°C and T= 33.5 °C) it is clearly deformed. At T= 33.5 °C with a laser power set to 190 mW the vesicle already seems to be affected by the trap in a similar way as at 500mW for T=22.4 °C. At 293 mW we can see undulations of the membrane. These are very quick fluctuations with big amplitude that can lead to the rupture of the membrane if the trap is kept switched on for more than a few seconds. These fluctuations were much weaker at 500 mW and T=22.4 °C. At T= 29.5 °C the vesicle seems to be in some intermediate state where it is affected more than at T=22.4 °C, but a little less than at T= 33.5 °C. Signs of deformation are visible at 260 mW and fluctuations of the membrane appear at 293 mW. The melting temperature of the binary lipid mixture DMPC/DPPC 50:50 was found to be T_m = 30.4 °C (see section 4.1), so image series E et F were taken of the vesicle being in the phase transition and series D shows the vesicle at a temperature just below phase transition. Since series E and F show greater deformation at lower laser powers this could be a first indication of an increased elasticity of the membrane at the phase transition or at least a clear temperature dependence. In the next subsection we will try to quantify these shape changes in order to compare the deformation of GUVs at different temperatures in a more accurate way.

A few relevant observations could still be made just by looking at the images and video photage of the experiments. We observed the following effect of a laser trap on giant vesicles:

• The bottom ITO was covered with a lipid film from which the vesicles grew during electroformation, so the vesicles were likely to be connected to the whole surface and in some sense to each other. This was comforted by the following observation. When the optical trap was focus randomly on the ITO surface all the vesicles around that spot were affected, see figure 25. This was observed up to 20 μm away from the trapping region or at least at distances much larger than the diameter of the trapping region (approximately 1 μm in diameter). The vesicles might even have been connected by small tethers, too small to be seen (see section 2.2.3 on electroformation). The mechanisms likely to affect the lipid membrane will be discussed in more detail in the Discussion.

We will now focus on the effect of the laser trap on single vesicles.

• As said before, the focus of the laser beam was set at approximately one third up from the base of the half-spherical vesicles. When the trap was turned on the observed deformation was instantaneous. Also the return to the resting shape was immediate once the laser was switched off.

• Two different types of deformation could be seen. At intermediate laser powers the vesicle shape changed slightly, usually as a small increase in the diameter of the observed cross-section. But at high powers the membrane underwent major shape fluctuations that stopped only once the trap was switched off.

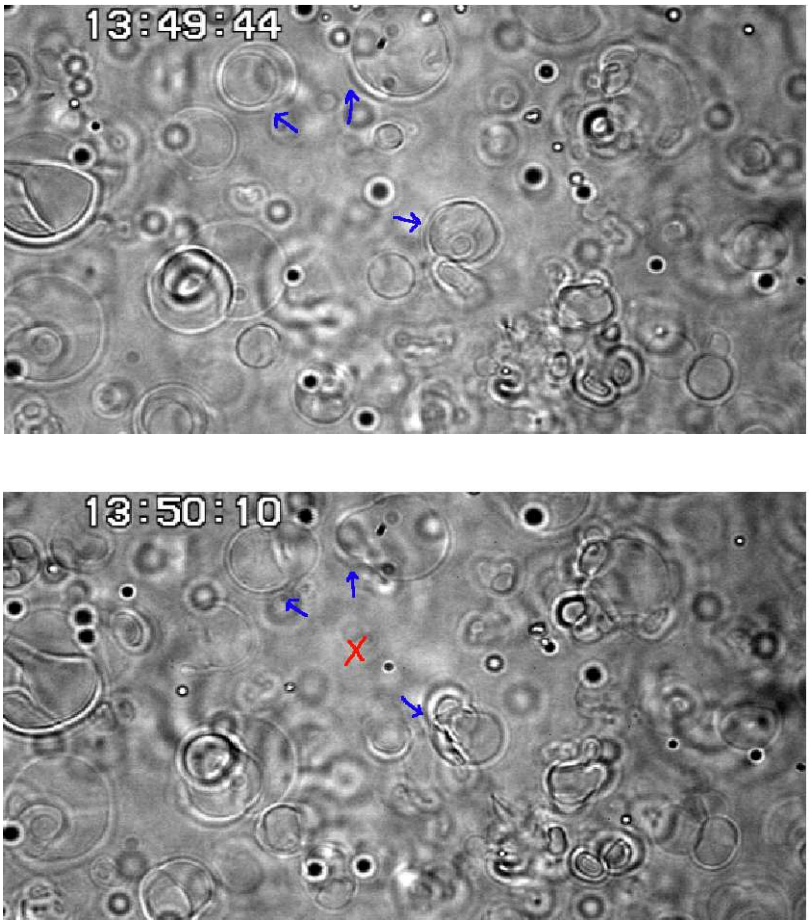

Figure 25: DMPC/DPPC 50:50 vesicles in brightfield. Influence of the laser light on the whole lipid film. Top: laser trap off. Bottom: laser trap on with a power of 326mW. The red mark shows the position of the trap. The blue arrows point out changes in vesicle shape.

• At temperatures corresponding to the main phase transition, the GUVs deformed at much lower laser powers than for temperatures below and above.

• At temperatures corresponding to the liquid-disordered phase, thermal fluctuations could be observed in the membrane without the laser being on. Still GUVs in the liquid-disordered phase were less affected by the laser trap than GUVs in the main phase transition.

• A vesicle deformed differently depending on where the trap was focused. The trap seemed to "push away" the part of the membrane that was the closest. See figure **??**.

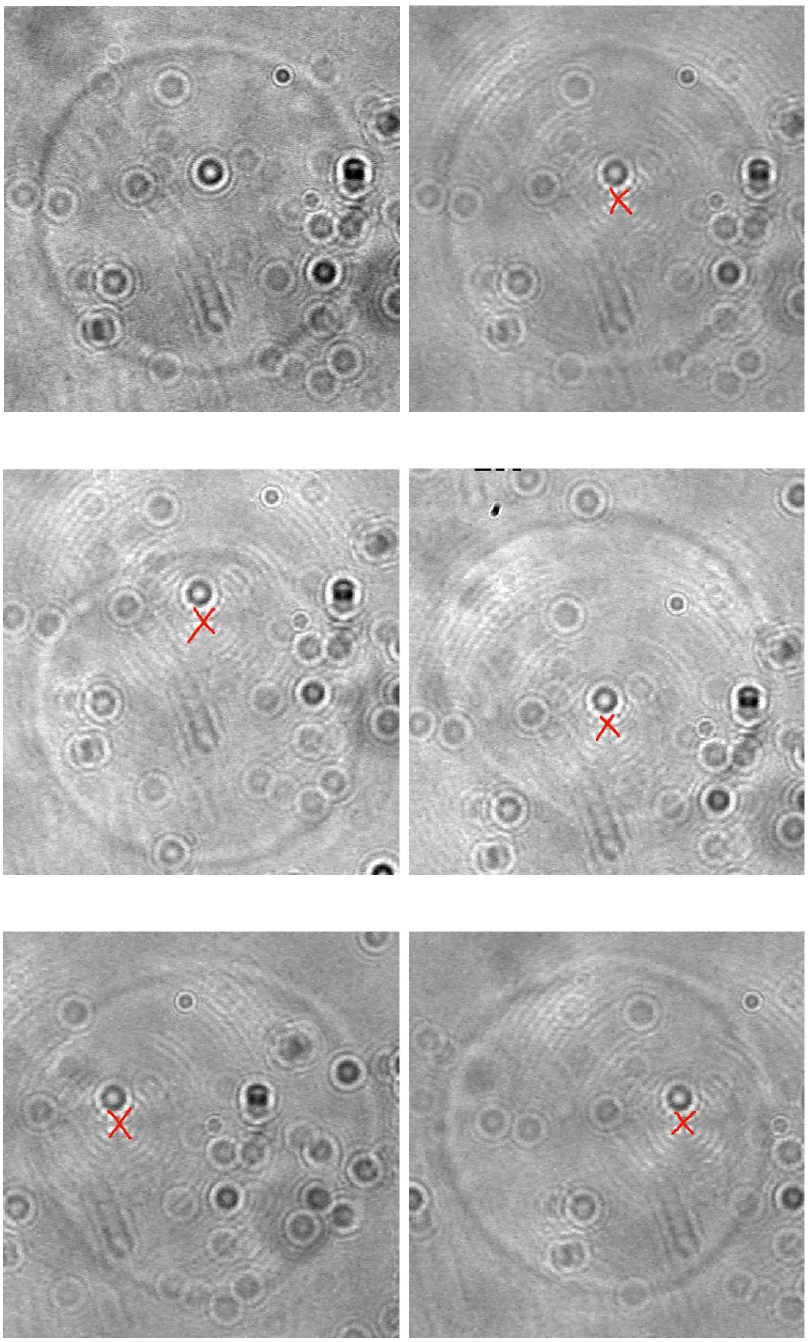

Figure 26: GUV deforming differently depending on the location of the optical trap. Top left: Laser off . Top right: Trap centered . Middle left: Trap in "upper" part of the vesicle . Middle right: Trap in "lower" part of the vesicle . Bottom left: Trap in "left " part of the vesicle . Bottom right: Trap in "right" part of the vesicle. The red marks show the position of the trap.

Another possible observation that needs further investigation was that under certain conditions the trapped vesicle first showed an instantaneous deformation as described before, but then also a second one at a much lower rate (maybe some sort of relaxation process)were the vesicles seemed to become even rounder. This was observed at intermediate laser powers, between the ones just slightly affecting the membrane and the ones deforming it heavily and at which fluctuations appeared.

4.3.2 Let's try to quantify

There are many ways of trying to quantify the deformation of a vesicle. We chose to calculate the ratio between the circumference (C) and the area (A) of a cross-section of the studied vesicle. We plotted C/A versus output laser power for each studied temperature, both for DMPC/DPPC 70:30 and DMPC/DPPC 50:50. How the data was fitted is described in the Data Analysis chapter. The smaller the ratio C/A the more circular the vesicle cross-section, since a perfect circle would minimize it.

Looking at the plots for DMPC/DPPC 70:30 (See figure 27), two different deformation regimes can be distinguished. First the ration C/A is approximately constant. This means that the degree of deformation is constant. After reaching a certain laser power that we chose to call the critical power (P_c) (the intersection of the two tangents of the fitted curve), a steep increase in the ratio can be seen, hence an increase in deformation. The laser powers above P_c are those at which big fluctuations of the membrane could be observed.

DMPC/DPPC 50:50 also shows this kind of behavior (See fig. 28). But here we seem to observe a slight decrease in the C/A ratio before getting into the second deformation regime. This is especially clear for series D at T = 22.4 °C. At that temperature the membrane is mainly in the solid-ordered phase and is thus a bit stiffer than a membrane in the liquid-disordered phase. We observed that vesicles at temperatures below the phase transition, without any laser being on, did not have a perfect spherical shape. The initial decrease of the ratio could be explained by the cross-section of the vesicle first getting rounder when exposed to the optical force, the kinks of the membrane being sort of pushed out.

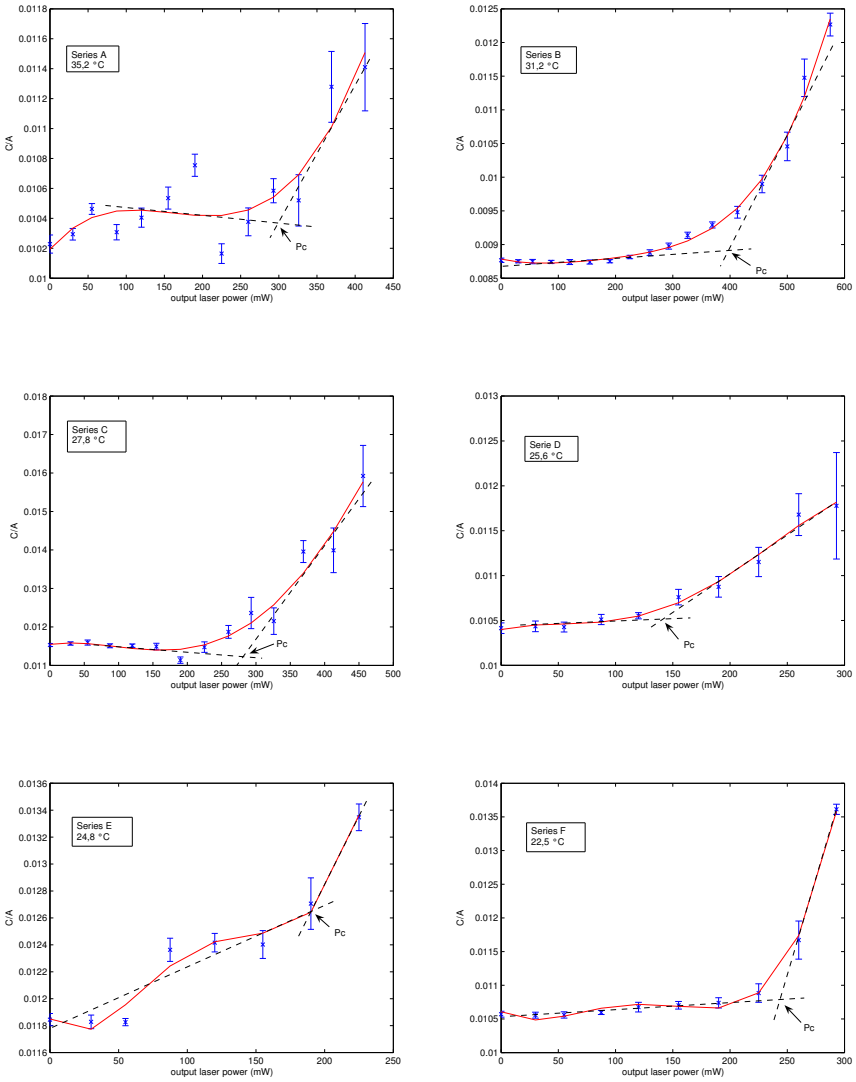

Figure 27: C/A versus output laser power for a DMPC/DPPC 70:30 vesicle at temperatures T_A=35.2 °C, T_B=31.2°C, T_C=27.8°C, T_D=25.6°C, T_E=24.8°C and T_F=22.5°C.

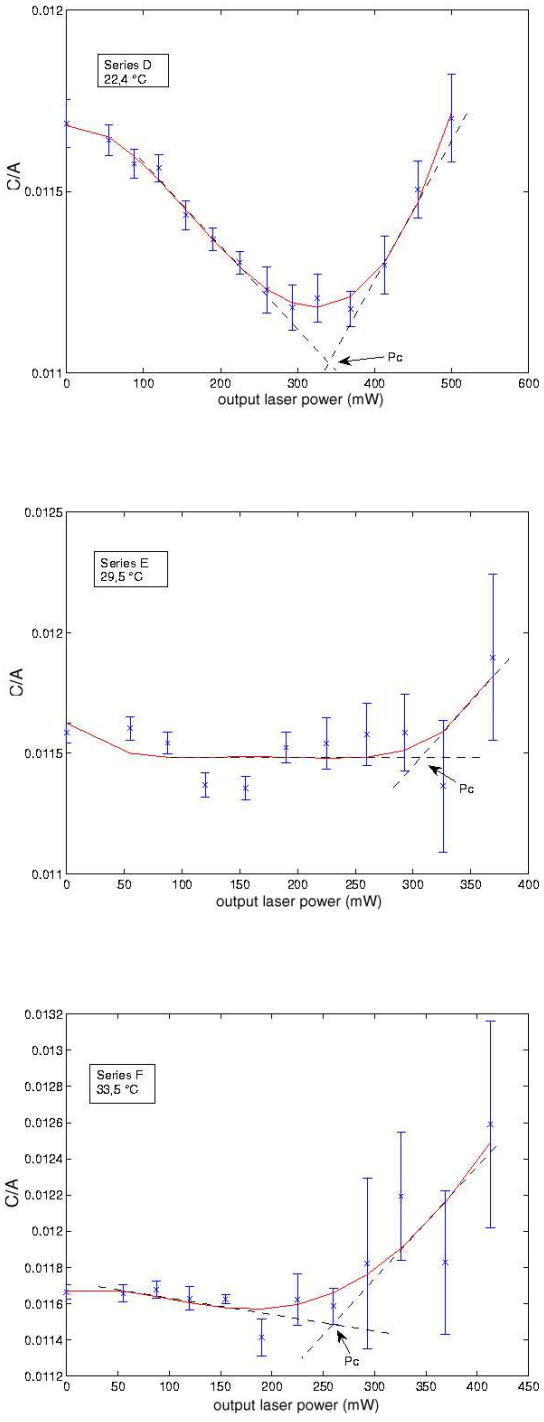

Figure 28: C/A versus output laser power for a DMPC/DPPC 50:50 vesicle at temperatures T_D=22.4°C, T_E=29.5°C and T_F=33.5°C.

In the table below we can see the values of the critical power (P_c) for every lipid composition and temperature.

Series	Lipid composition	temperature (°C)	P_c (mW)
D	DMPC/DPPC 50:50	22.4	341
E	DMPC/DPPC 50:50	29.5	306
F	DMPC/DPPC 50:50	33.5	260
A	DMPC/DPPC 70:30	35.2	299
B	DMPC/DPPC 70:30	31.2	399
C	DMPC/DPPC 70:30	27.8	280
D	DMPC/DPPC 70:30	25.6	145
E	DMPC/DPPC 70:30	24.8	190
F	DMPC/DPPC 70:30	22.5	244

4.3.3 Comparison with calorimetry results

In figures 29 and 30 we plotted the critical power together with the Cp-profiles of the concerned lipid mixtures. The y-axis for P_c was scaled so that its highest value approximately corresponds to the maximum value of the Cp-profile. These graphs don't show a quantitative relation between heat capacity and critical power, but show a correlation between an increase in heat capacity in the studied system and a decrease of the laser power needed to deform the vesicles. This would mean that in the main phase transition lower laser powers are needed to deform a lipid membrane, i.e. the membrane is easier to deform. It isn't a perfect fit but the tendency is quite clear. In figure 29 the P_c values of series B, C, D and E correspond quite well to the Cp-curve. From our predictions the P_c values of series A and F should be higher, but $T_F = 22.5$ °C and $T_A = 35.2$ °C are close to T_s and T_l of the DMPC/DPPC 70:30 phase transition and some phenomenon related to phase fluctuations close to the phase transition boundaries could be imagined. We would need to make several measurements at the same temperature to get a better idea of what happens. Still the higher powers needed to deform series B in figure 29 and series D in figure 30, being just at the phase boundary, would support the hypothesis of a lower deformability at temperatures below and above the phase transition.

Complementary investigations on vesicle deformability at temperatures further away from the phase transition would be necessary before any definitive conclusions can be drawn. One problem that this may cause is that the more the temperature differs from room temperature the harder it is to reach it inside the sample chamber (see fig. 16). To reach 15 °C we would need to go below the recommended working temperature of the objective. The same goes for temperatures above 40 °C. It can both damage the objective and cause a loss in image quality, since the objective is corrected for optical aberrations for near room temperature conditions. The use of an air objective would solve the heat loss problem, but they never come with a NA greater than 1, making it difficult to trap objects bigger than 3 μm (personal communication, Nader Reihani). This might work for trapping membranes.

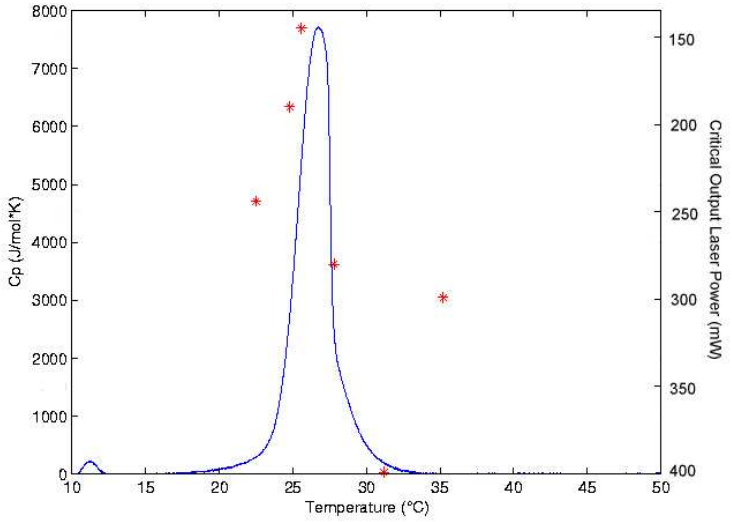

Figure 29: Critical power (red dotes) and heat capacity (blue line) versus temperature for DMPC/DPPC 70:30.

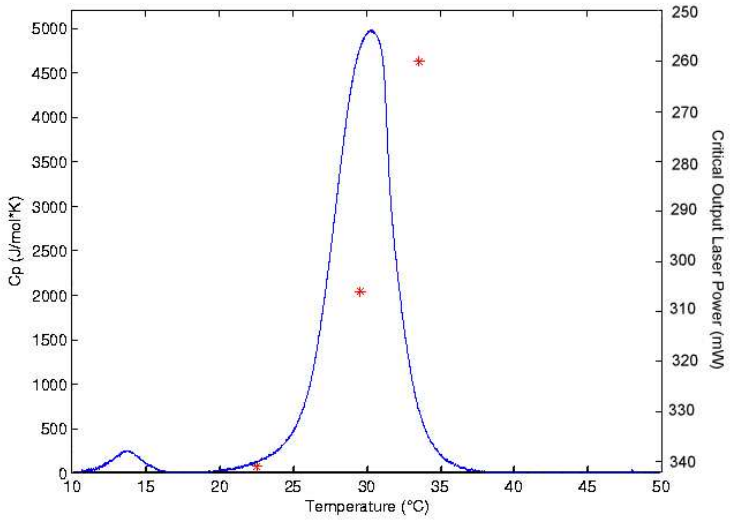

Figure 30: Critical power (red dotes) and heat capacity (blue line) versus temperature for DMPC/DPPC 50:50.

We calculate the ratio between the critical power outside and inside the phase transition. For DMPC/DPPC 70:30 we took the P_c value of series D divided by the P_c value of series A. This would suggest that the membrane is approximately two times (2.06) easier to deform in the phase transition regime. We could also use P_c of series B instead of A. The laser power needed to deform the vesicle heavily would then be 2.77 times larger outside the phase transition than inside. For DMPC/DPPC 50:50 the corresponding number would be 1.33.

It has been shown that the bending modulus of lipid membranes do depend on temperature [74][67]. The question is whether we can use the change in P_c to estimate the bending modulus of the lipid membrane in the main phase transition. Knowing that the value of the bending modulus of DMPC in the fluid phase is of $\kappa_B = 1.1 \times 10^{-19}$J at $T = T_m + 2.5°$ [43] could we just assume its value is approximately twice as high for temperatures corresponding to the phase transition? We will discuss this further in section 5.2.2.

5 Discussion

5.1 Optical Tweezers and lipid membranes

5.1.1 Observations in publications

There are not many reports on giant unilamellar vesicles being deformed directly by optical tweezers. Instead they are often used as a tool to grab vesicles and stabilize them in order to make other kinds of experiment. The lack of observed deformations could be explained by the fact that most of these experiments take place at temperatures outside the phase transition and at powers just below what is critical for a GUV outside the transition regime.

Cherney et al. [44] have investigated the effect of optical forces on the shape of unilamellar DPPC vesicles both in solution and adhered to a coverslip using confocal-Raman microscopy.

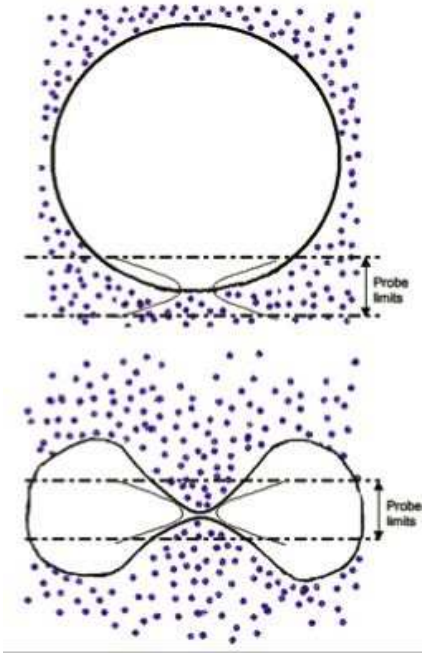

Figure 31: Cartoons depicting one and two bilayers in an optical trap. The dots represent the perchlorate ions in the solution outside the vesicle . They were used to monitor the relative amount of buffer solution outside the vesicle within the confocal probe volume marked by the horizontal dashed lines. This gives an indication on the shape of the trapped vesicle.[44]

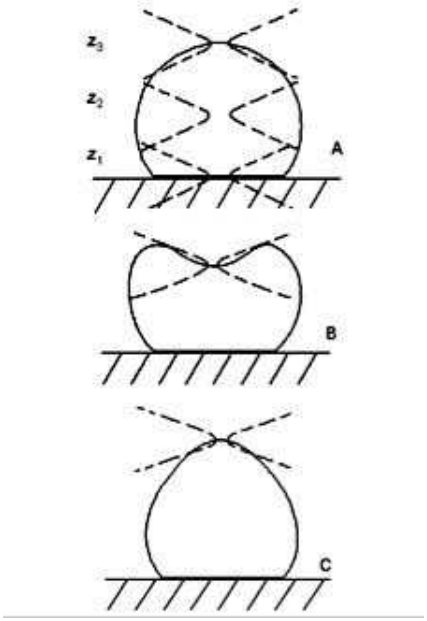

Figure 32: Shapes of surface-attached liposomes in response to the forces of an optical trap. A) Cross section of a rigid liposome (hydrated in the presence of calcium ions) that doesn't respond to optical forces. B) Cross section of a liposome with the focus of the trapping laser inside the liposome. C) Cross section of a liposome with the focus of the trapping laser above the equilibrium position of the bilayer.[44]

In these experiments the 647.1 nm line from a Kr^+ laser was used both to trap and to make a Raman scattering analysis of unilamellar DPPC vesicles with a diameter of 3 to 5 μm. The confocal design of the microscope made it possible to distinguish the inside of a vesicle from its outside. The maximum laser power at the focus was 30 mW. Even at 6 mW the vesicles showed signs of deformation. A jump in the amount of phospholipid and perchlorate ions within the optical trap could be measured. This could indicate that a second bilayer was drawn into the center of the trap (See figures 31 and 32).[44] 6 mW is quite low compared to the laser power we needed in order to see any change of the vesicle shape. On the other hand we only looked at a xy-cross section of the vesicles and couldn't visualize the actual 3D shape of the membrane. They also used an other wavelength and worked with smaller vesicles. Still this shows a similar phenomenon to what we could observe. Lipid membranes seem to be affect by optical forces.

Another quite extensive study has been made with a 488-514 nm Argon laser on GUVs by Bar-Ziv et al. [45][46][47]. They report of spontaneous vesicle expulsion following exposure to optical tweezers. The laser was focused for a few minutes with low power on the lipid membrane, pressurizing the vesicle and making it tense. For a single unilamellar vesicle this effect could last long (hours) after

the laser had been switched off. Their hypothesis in explaining spontaneous expulsion is that the laser trap pulls lipids out off the bilayer and that a colloid suspension forms between the inner and the outer vesicles giving rise to an osmotic pressure. The outer membrane has to be tense in order for the vesicle expulsion to take place. The two vesicles can be of the same size. Also expulsion under constant tweezing has been observed. During these experiments the studied one-component 10 μm vesicles (DMPC, DOPC and other uncharged lipids) were in the liquid phase.

Laser-induced tension drops significantly with wavelength:

$$\Sigma_L \propto \frac{1}{\lambda^2} \tag{16}$$

where Σ_L is an upper limit on the tension that could be induced in the membrane and λ^2 is the wavelength of the laser light [47]. Vesicle expulsion might therefore be difficult to observe using a 1064 nm laser, at least more than sporadically. Our observations at intermediate laser powers, at which some vesicles showed a second deformation at a much slower rate (see section 4.3.1), might correspond to a laser-induced tension in the membrane. The cross-section of the vesicles seemed to become rounder. This took place while the laser was still on.

5.1.2 Laser induced heating

Using near-infrared lasers for optical trapping reduces nonthermal photodamage of biological materials. We will get back to that in section 5.1.4. Now we will concentrate on the heating effect of highly focused laser beams. Heating of the sample by the trapping laser increases thermal motion of the trapped particle and decreases the viscosity of the medium [48]. What is the extent of laser-induced heating by a 1064 nm laser? Could it be even partially responsible for the observed deformations?

Liu et al. [49] measured temperature changes by observing phase transitions in membranes. One component 10 μm liposomes were labeled with Laurdan, a dye probe sensitive to temperature. The dye was excited by a UV beam (365 nm). With the absorption of infrared radiation from the trapping beam (Nd:YAG laser, 1064 nm), temperature increased in the sample and at the melting temperature a phase transition from gel to fluid phase occurred in the lipid membrane. This transition was accompanied by a large Stokes shift in the fluorescence emission of the dye. From that they could derive the generalized polarization (GP) as a function of temperature.

$$GP = \frac{(I_g - I_l)}{(I_g + I_l)} \tag{17}$$

where I_g and I_l are the fluorescence intensities measured at the maximum emission wavelengths of Laurdan when the membrane is in the gel respectively fluid

phase. For a one component lipid membrane the transition peak is very narrow so the corresponding slop in GP is very steep. A calibration curve was made by measuring GP versus temperature for a free liposome. From the laser-induced change in GP they could then get the temperature change as a function of laser power. For laser powers up to $\sim$ 300 mW the temperature change was seen to be linearly proportional to the applied power. For liposomes a heating rate of $\approx 1.45 \pm 0.15\,^{\circ}\mathrm{C}/100\,\mathrm{mW}$ could be measured. [49]

Studying the heating effect on live cells is trickier with this method since their membrane doesn't show a distinct phase transitions. Cellular GP measurements are therefore less sensitive to small temperature changes, but on the other hand it is possible to quantify the localized heating over a larger temperature span. For Chinese hamster ovary (CHO) cells a heating rate of $\approx 1.15 \pm 0.25\,^{\circ}\mathrm{C}/100\,\mathrm{mW}$ was measured.[49] For live sperm cells they found a corresponding rate of $\approx 0.92 \pm 0.70\,^{\circ}\mathrm{C}/100\,\mathrm{mW}$ [50].

More recently Peterman et al. [48] have measured heating induced by a 1064 nm laser when trapping silica and polystyrene beads in different media. According to their model the biggest contribution to heating is the absorption of the laser light by the solvent which is much larger then the heat absorption by the trapped particle itself. Heating both increases the thermal motion of particles and decreases the viscosity of the medium, so they measured the temperature changes in the focus of a laser trap by analyzing the Brownian motion of a trapped bead. For 500 nm silica beads in water they measured a temperature increase of $7.7 \pm 1.2\,\mathrm{K/W}$ and slightly more for a 444 nm bead ($10\,\mu\mathrm{m}$ from the glass-solvent interface). To demonstrate the importance of the surrounding medium, trapping a polystyrene bead of the same size in glycerol gives a temperature increase of $42.2 \pm 0.5\,\mathrm{K/W}$.

All laser powers given so far in this section are laser powers near the trap focus. The results of Liu et al. span between 14.5 K/W for liposomes and 9.2 K/W for sperm cells. This is a slightly higher heating effect than the one measured on beads by Peterman et al. (between 7.7 and 8.1 K/W). Although they worked on silica and polystyrene beads they estimate that their results can be generalized. They have shown both experimentally and in their model that the contribution of the trapped particle to the heating is quite small. In addition to that the heat conductivity and absorption coefficient for water and lipids are quite similar making heat confinement inside a cell or a lipisome rather unlikely. So the two results should be comparable. One possible explanation of the discrepancy is that in the experiments of Liu et al. the medium was not pure water. Wurlitzer et al. measured a temperature change of $\approx 5\,\mathrm{K/W}$ in the focus when making optical tweezers experiments at the air/water interface of Langmuir-monolayers [51]. This is also quite consistent with the other results considering it is an other type of system. Assuming Peterman's results are the most accurate we would get for most optical tweezers experiments (100 mW near focus, 160 mW output laser power) a temperature increase of 0.8 K.

When estimating the temperature rise of samples in our experiments the cooling effect of the bottom ITO should also be considered. The laser induced heating corresponding to a 502 nm polystyrene bead trapped in glycerol was measured to $55.3 \pm 1.5\,\mathrm{K/W}$ and $37.0 \pm 1.8\,\mathrm{K/W}$ for a distance between the focus and the glass surface of 20 respectively $2.5\,\mu\mathrm{m}$ [48]. During our experiments the trap was focused 10 to $5\,\mu\mathrm{m}$ from the ITO surface. The cooling effect might be less dramatic in water, but should still be taken into account. Our measurements of the temperature fluctuations during experiments are consistent with the above reported results, although not as precise since the used thermocoupler wasn't placed exactly in the trap focus. Once using the objective heater we observed temperature changes of 0.1 to $0.2\,^{\circ}\mathrm{C}$. Measured changes were never bigger than half a degree. The maximum output laser power we used was 575 mW (350 mW at the focus assuming the same objective transmission of 62% at $\lambda = 1064\mathrm{nm}$ as in [48]). According to Peterman's results this would correspond to a maximum laser-induced heating of $2.8\,\mathrm{K}$.

The heating-induced change in viscosity should also be considered as a potential source of error and should be taken into account when calibrating the trap stiffness [48]. Could the change in viscosity also affect the observed shape fluctuations in our experiments? Thermal fluctuations were observed at temperatures above the phase transition, but they were smaller then the laser-induced fluctuations observed at temperatures corresponding to the transition itself. It is hard to say if the change in viscosity of the surrounding medium has a quantitative effect, but at least it does not seem to be qualitative.

Assuming water as the solvent, laser-light absorption has a small but measurable heating effect. This is not likely to be the cause of the shape fluctuations observed in our experiments but should be taken into account even in the near-infrared region when doing optical tweezers experiments.

5.1.3 Dielectric constants

Now that we have excluded laser induced heating as the source of deformation we can work under the hypothesis that the optical force exerted by the optical tweezers affects the membrane.

Despite the 5nm thickness of the lipid bilayer, which is much smaller than the wavelength of 1064nm of the laser, the GUVs are directly affected by the light and the membrane is deflected into the focus of the trap (see section 5.1.1). One of the observations made during our experiments would support this. Vesicles deformed differently depending on the position of the trap focus within the vesicle (see figure 26). This would suggest that the membrane really is pulled into the focus of the trap.

There is a large difference in dielectric constant between the surrounding water and the lipid membrane. At $20\,^{\circ}\mathrm{C}$ water has a dielectric constant of 80.1 [53] and at room temperature a lipid bilayer has a dielectric constant of 2 to 10 [52]. This is comparable to the one of a polystyrene bead which has a dielectric

constant of 2.4 to 2.7 [53]. The relative dielectric constants mentioned in this paragraph are defined as follows:

$$\varepsilon_r = \frac{\varepsilon_s}{\varepsilon_0} \tag{18}$$

where ε_s is the static permittivity of the material and ε_0 is the vacuum permittivity [53]. The lower the dielectric constant the better the dielectric [55].

This big difference in dielectric constant between the lipid membrane and the surrounding medium can be related to the difference in refractive index by the following expression:

$$\varepsilon_r = m^2 \tag{19}$$

where m is the complex refractive index $m = n - ik$. If we only look at the real part of both the dielectric constant and the refractive index we get $\varepsilon_r = n^2$.[56] So a big difference in dielectric constants between the lipid membrane and the water corresponds to a difference in refractive indexes. This in turn gives a change in the momentum carried by the light and the membrane is imparted a momentum change in opposite direction. The membrane is subsequently deflected towards the center of the trap were the light intensity is the highest (see section 2.3.1).

Worth mentioning is that a lipid bilayer can almost be regarded as a 2D surface. In the xy-plan, within the trapping volume, its size is comparable to λ, but in the z-direction the thickness of the bilayer is much smaller than λ. This would corresponds to the Rayleigh regime (see section 2.3.1). But even if the trapping process is more complex than described above, lipid membranes can be trapped by optical tweezers.

5.1.4 How could the laser affect live cells?

The GUVs we studied are comparable in size to cells. Procaryotic cells have a size of approximately 1 micron [57] and the size of eucaryotic cells lies between 10 and 100 microns in diameter [58], but most cells are much more rigid than GUVs. The cytoskeleton, an eventual outer membrane as for E. coli or yeast, densely packed organelles prevent the plasma membrane from deforming heavily. Although, red blood cells show a quite different behavior. They are different from other cells in that they don't have any nucleus or organelles. Their cytoskeleton also has fewer points of anchoring to the plasma membrane. This allows them to deform easily in order to squeeze through small capillaries.[59] Optical tweezers studies have been made on that subject. Even if they do not deform cells should feel if a force is acting on their membrane. It is hard to assess the actual effect this could have on cell function, but it seems unlikely that this wouldn't put the cell under some sort of stress.

The membrane isn't the only part of a cell potentially affected by a focused laser beam. One way to investigate the damage caused by optical tweezers is to monitor specimen physiology during trapping. The viability of the studied cells can be assessed by looking at motility [61], rotation rates of flagellar motors [63], cloning ability [60], cell death [50]. We will look at the wavelength, exposure time and power density dependence of these biological functions.

The wavelength dependence of photodamage in E. coli doesn't show any similarity to the absorption spectrum of suspensions of E. coli cells, to water absorption or to the absorption of molecular oxygen. Light could be absorbed by one or more specific photopigments. There is a resemblance though with photodamage in Chinese hamster ovary (CHO) cells (see figure 33).[63] From the collection of data shown in the table on next page, the most damaging wavelengths seem to be 740 to 760 nm and around 900 nm. This corresponds to wavelengths twice those of the fluorescence excitation maxima of free NAD(P)H and flavins [62]. 800 to 850 nm seems to be a quite good wavelength range to use, at least looking at the reported parameters. 1064 nm was good overall except for cloning efficiency at longer exposure times. 950 to 990 nm was the optimum wavelength interval to work in when looking at cloning efficiency. It also gave little damage to E. Coli cells, but we don't have as much data as for 1064 nm.

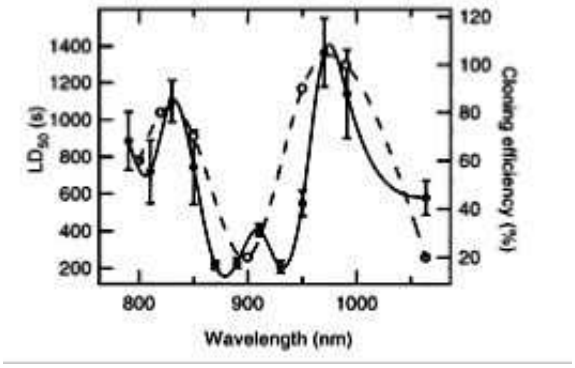

Figure 33: The wavelength dependence of photodamage in E. coli plotted as LD_50 data for a laser power of 100 mW (dashed line, open circles) compared to CHO cells (solid line, solid circles). The data on CHO cells' cloning efficiency [60] was determined after 5 min of trapping at 88 mW. [63]

Wavelength (nm)	Cloning efficiency (exposure of the nucleus) [60]	Viability and motility of sperm cells (autofluorescence) [61]	Colony forming (size and number of cells) [62]	Rotation rate (E-coli) [63]
670-680			No damage at laser powers high enough to trap beads (2min exposure)	
700	poor $<$ 40% exposure times $\geq 5min$			
740-760	minimum 0-20%	big change within 1min, reduced motility, paralysis, viability loss		
800-850	good 50-90% exposure times $\leq 3min$	No change after 10min exposure, no viability loss		Least damage
870				Most damage
900	poor $<$40% exposure times $\geq 5min$			
930				Most damage
950-990	optimum 60-100%			Least damage
1064	poor $<$40% exposure times $\geq 5min$	No viability loss	No damage at laser powers high enough to trap beads (2min exposure)	Twice the sensitivity of 830 and 970 but no major damage

The table above shows the wavelength dependence of a few cellular functions.
No data was available for the empty entries.

Duration of exposure also plays an important role in the extent of the damage inflicted to a cell. For 1064 nm lasers, three minutes of exposure at a laser power of 176mW in the trap focus reduced the cloning efficiency to 30% . With an exposure time of one minute a 90% cloning efficiency was reported. So for short exposure times to a 1064 nm laser the viability of CHO cells is hardly altered.[60] A nearly linear decline in the average of the normalized rotation rate with time was found for all investigated wavelengths and laser powers. This would suggest that photodamage is a gradual process with no apparent threshold [63]. It would also be interesting to find out if there is a cumulative effect. Do short but repeated exposures induce any photodamage?

How much damage a certain laser power induces also depends on the size of the focal spot [62], which means that what is actually crucial is the power density. The higher the power density, the higher the photodamage. Some data is also reported as energy densities which is defined as power density multiplied by exposure time and usually given in J/cm^2 [60].

For E. coli grown anaerobically there was a three- to sixfold increase in the time (LD_{50}) at which the rotation rate of the bacterium decreased with 50%. This suggests a critical role for oxygen in the damage pathway. It isn't clear if oxygen is directly responsible for the damage or if it triggers some other process. [63]

In Neuman et al. [63] the sensitivity is defined as the reciprocal of the lifetime. For wavelengths of 870 and 1064 nm they found that the sensitivity of cells was linearly related to the intensity, hence to laser power. This suggests that a single-photon process leads to photodamage in the infrared region. On the other hand two-photon processes have been reported in the visible light range [50][61].

Also the type of laser used plays a big role in the extent of the photodamage induced by the trapping. Results from continuous wave (cw) trapping at 1064 nm seem to support the conclusion that infrared laser tweezers do not induce significant physiological changes in trapped cells [50] (see also the table on the previous page). Pulsed lasers produce a transient temperature increase that was found to facilitate DNA denaturation processes. They might also induce two-photon damage processes.[50] Multifrequency cw lasers like Ti:Sapphire lasers can give rise to unstable light pulses. Their intensity was the highest at a wavelength of 760nm.[61] This might explain the high degree of photodamage at that particular wavelength reported by both König et al. [61] and Liang et al. [60] since both groups used this type of laser. Also Neuman et al. [63] did so, but at higher wavelengths. Interesting to notice is that 1.5 mW irradiation at 365 nm (UVA), with a 50 W high pressure mercury lamp often used in fluorescence microscopy, was enough to cause the paralysis and subsequently the death of the exposed sperm cells [61].

All these processes are quite different from the vesicle deformations we observed. It would be interesting to find out if an eventual stress on the plasma membrane could have any additional effect on cell viability. In conclusion, optical trapping with a continuous wave 1064 nm laser induces little photodamage as long as the exposure time and the laser power are kept moderate.

5.2 Phase transition and membrane elasticity

5.2.1 Increased elasticity and cell functions

At the main phase transition between the solid-ordered and the liquid-disordered phases we observed the existence of domains at the surface of DMPC/DPPC GUVs which would suggest a phase separation. This has been shown by many groups [10][65][28][42]. We have also shown an increase of the elasticity of the lipid membrane for the corresponding temperature interval. Are these two observations linked? The bending of a bilayer involves both a stretching of one of its leaflets and the compression of the other [7]. So the lipids in the outer leaflet need to occupy a larger area than when the membrane is at rest and the lipids in the inner leaflet need to occupy a smaller area. Upon melting lipid membranes show an area increase of 20 to 25% [43][74]. This is due to the increase of the orientational disorder in the hydrocarbon chains of the lipid molecules. If the lipid membrane can rearrange so that locally, when bending, the outer monolayer contains more lipids in the fluid phase and the inner monolayer is composed of more lipids in the gel phase, then it should be easy to deform. Lateral diffusion in bilayers is already quite quick, in the range of nanoseconds, especially in the fluid phase [4]. Additionally, at the phase transition, the lipid molecules can go from the ordered to the disordered configuration and vice versa without having to overcome any energy barrier. This could explain the increase in elasticity. In the phase transition it costs less to bend the membrane than outside. It is not only the melting transition that has an effect on membrane bending elasticity. The inverse is also true. Since shifting the outer monolayer's transition to lower temperatures and the inner monolayer's transition to higher temperatures, bending of the membrane will alter measured heat capacity profiles by broadening them [43].

Baumgart et al. [64][65] have studied the coexistence of liquid-ordered (L_o) and liquid-disordered (L_d) domains. Vesicles with coexisting fluid phases have shapes and domain morphologies distinctly different from vesicles with gel/fluid phase coexistence. Fluid domains tend to minimize their boundary perimeter due to line tension. Above some limiting boundary length a spherical bud forms, which can lead to fission. In [65] the correlation between domain composition and local membrane curvature is shown by two-photon fluorescence microscopy. Vesicles with gel and fluid domains don't show these big differences in curvature between the two phases. Their domains have irregular shapes giving rise to an elongated boundary.[64] Curvature can play a big role in biological functions, especially curvature changes like for example in cellular trafficking events such as pinching off of endocytic vesicles, fusion, budding or tubulation [66]. Highly curved membranes are found in functionally distinct regions of the plasma membrane such as microvilli, secretory vesicles, parts of the endoplasmic reticulum and the Golgi apparatus [64]. Domains could also have a function as signaling platforms, containing proteins or producing lipids and different messenger molecules. Phase percolation is then a highly relevant idea to discuss. If we assume that a membrane is made of two coexisting phases from which one has its domains interconnected. Molecules having higher affinity to that particular

phase could then diffuse around freely through the whole membrane. The other phase is then dispersed in delimited domains. A change in temperature or composition can trigger a shift in which of the phases that is percolating. Of course both phases can be percolating to various extent at the same time.[66] Lipid domains are not static. They can expand and migrate around the membrane surface. Their motility though is dependent of temperature. The more the temperature is reduced the less they move. [42] In other words the lipid membrane is in constant rearrangement. In order to control biological processes linked to both curvature and domain repartition, the cell has to have mechanisms controlling the lipid composition of its many membranes. Sorting mechanisms by vesicle or tubule budding and enzyme activity are at least two of the ways in which the cell does this [66]. Phase separation seems to play a significant role in biologically relevant processes. This could imply that the closeness of the melting temperature of biological membranes to biologically relevant temperatures, such as body temperature or growth temperature, isn't just a coincidence.

5.2.2 Other techniques used for measuring membrane elasticity

A wide range of more or less invasive techniques are used to determine the elastic properties of lipid vesicles and cells. Spectral analysis of shape fluctuations can be used, but only to determine the bending modulus of membranes in the fluid phase. With micropipette aspiration it is possible to measure both surface compressibility and the bending modulus of a bilayer. However the probable coupling in the gel phase between the two monolayers makes the estimation of the bending modulus more difficult. The method is therefore mostly used for determining elastic properties of membranes in the fluid phase.[67] Also micropipette electrodes have been used. Since electroporation is induced by large electric fields (kV/cm), optical techniques with a very high resolution are needed to resolve the submicrometer deformations induced by a smaller field. This was done by using differential confocal microscopy [70]. In the fluid phase electrically driven deformations were not observed since the membrane motion was dominated by thermal fluctuations.[68] GUVs have also been shown to deform under the influence of dielectric force potentials. The forces induced by the used octode dielectrophoretic field cage are well known and could be used to determine the bending modulus of the trapped GUVs.[71]

Optical tweezers can be used as a way of stabilizing vesicles in combination with an other method. Foo et al. [72][73] used a 1064 nm laser at an output laser power of 200mW to trap DPPC and DMPC 10 μm unilamellar vesicles (ULVs). According to them this gave the trapped vesicles a more elongated shape. The ULVs were then subjected to different fluid flow velocities at different temperatures and the resulting deformations were monitored. As we did, they observed a correlation between the deformability of the vesicles and the phase transition. They also give an estimation of the deviation of the drag force from the predictions made in the case of a trapped rigid sphere. This method is unlikely though to give any accurate quantitative data on the elasticity of lipid vesicles.

Lee et al. [67][69] used optical tweezers together with differential confocal microscopy (for the method see [70]). This gave nanometer depth resolution of the monitoring of the deformations induced by the the optical trap (532-nm beam, 45 mW laser power). To calculate the bending modulus κ_B they used the free energy density:

$$\Delta G_{bending} = \frac{1}{2}\kappa_B(\frac{1}{R_1} + \frac{1}{R_2})^2 + \frac{\kappa_G}{R_1 R_2} \tag{20}$$

Where κ_B is the bending modulus and κ_G is the Gaussian bending rigidity. We can neglect the Gaussian term since its integral is invariant under shape deformation within a given topology [7]. For each selected temperature they got κ_B from the difference in:

$$\Delta G_{bending} = \frac{1}{2}\kappa_B(\frac{1}{R_1} + \frac{1}{R_2})^2 \tag{21}$$

before and after deformation by the tweezers. For a sphere, which is approximately the case before deformation, the two curvature parameters R_1 and R_2 are equal. They then assumed that the trapped vesicle adopts an ellipsoid shape. This differs from what was observed by Cherney et al., but maybe for this low laser power the approximation is good enough. Using the integral version of the above equation they got the following expression for the bending modulus:

$$\kappa_B = \frac{2W}{\int_\Omega (\frac{1}{R_1} + \frac{1}{R_2})^2 dA - 16\pi} \tag{22}$$

where W is the work done by the optical force.

After calculating the new curvatures and estimating W they got κ_B for a particular temperature. This was repeated with an interval of two degrees for temperatures between 25 and 50 °C as to get the phase transition with good margins. In comparing their results for κ_B with data obtained by spectral analysis they found no major discrepancies.[69] However a few of their assumptions and simplifications are a little shaky. For example, it is not mentioned how they got the value of the work done by the optical force. We might have used some similar way of roughly estimating the bending modulus, but for higher laser powers, at which fluctuations of the membrane occur, this method wouldn't have been possible to use.

Dimova et al. [74] used an optical trap with two contrapropagating laser beams which each could be split into two parallel beams with a maximum distance between them of 35μm. The setup was fed by an 514.5 nm argon ion laser. The design of the trap allowed a lower laser power to be used, 6 mW inside the focus. This is quite low compared to powers needed for standard optical tweezing. They used micron-size latex beads to probe the viscous and elastic responses of

DMPC GUVs depending on temperature. For temperatures above the melting temperature ($T_m \approx 23.4\,^{\circ}\mathrm{C}$) they used three methods: sedimentation where a bead attached to the membrane was released close to the upper pole of the vesicle and glided down towards the lowest point, Brownian motion analysis and optical trapping dynamics where the trap was switched on a few micrometers away from the bead. For temperatures below the phase transition, corresponding to the gel phase, the double trap configuration was used on two beads, one being kept fixed. When the other trap was moved the membrane elasticity worked against an increase of the distance separating the two beads. Because the latex beads are macroscopic they did experience the large scale viscosity ν_s. At T_m, approaching from below, the elastic response of the membrane vanishes and it can be regarded simply as a viscous fluid. No viscoelastic behavior was detected in the fluid phase. Close to the melting temperature, approaching from above ($T \sim 23.3\,^{\circ}\mathrm{C}$), there was a drastic increase (approximately 5 fold) in ν_s that could be explained by pretransitional structure fluctuations and the formation of domains. From the experiments in the gel phase the membrane stiffness (k_M) could be deduced. Close to T_m there was a marked decrease in k_M, which corresponds to the earlier reported decrease in the elastic response. From that they could roughly estimate the curvature modulus. It was high in the gel phase, but close to the melting transition it decreased abruptly. It then increased slightly for temperatures just above the transition before planing out to a constant in the fluid phase.We should keep in mind that they mostly investigated the in-plane viscoelastic properties of a lipid bilayer and not the bending properties as we did. To our knowledge there is no direct way of measuring the bending modulus of lipid bilayers in the gel phase. Theoretical studies have been made [43], but won't be recollected here. In order to know whether we can estimate the change in bending modulus to be proportional to the decrease in C_p, we need to do further theoretical studies.

5.2.3 Is there really a critical power?

We did observe two different types of deformation, an instantaneous change from one fixed shape to another at intermediate laser powers and membrane fluctuations at higher powers. We chose to define the critical power P_c as a sort of threshold laser power at which the vesicles started to show dynamic shape fluctuations, but is this view really justified? First of all more data points are needed before we can make a more clear statement on the type of transition between the two deformation regimes. It is though more likely to be smooth.

We will now try to explain why heavy shape fluctuations could be observed. A first explanation that could come into mind is the eventual rupture of the membrane. This is not likely to be since the vesicles, if not exposed to the laser for too long, could recover their original shape. In the cases the membrane actually ruptured there was no ambiguity about it. There is another way of explaining this. The energy cost of increasing the membrane area is much larger than the free energy available from the optical trap [44]. By using the average permeability coefficient of water through a phospholipid membrane and following the calculations done by Cherney et al. [44] we could estimate the complete exchange

of the water inside a 20 μm half-sphere vesicle to take only 77 ms (it would be the same for a whole vesicle). This would mean that the vesicle deformation is accompanied by a volume decrease rather than an area increase. Assuming that the area to volume ratio before trapping was close to the one of a perfect sphere (or in our case a half-sphere) a decrease in volume would increase this ratio. A perfect sphere only has one possible configuration whereas an ellipsoid has many more configurations for a given area to volume ratio. This would explain why the membrane of a vesicle fluctuates when it is deformed by optical tweezers. It would also be interesting to repeat the experiments on whole vesicles in order to exclude or not the fact that we investigated half-spheres attached to the bottom ITO as the cause of the observed shape fluctuations.

Finding a plausible explanation for these fluctuations doesn't explain why they don't occur at lower laser powers at which the membrane is already bend by the trap and at which subsequently, the area to volume ratio is changed. Maybe some additional energy is needed for the fluctuations to occur.

Still the determination of a critical power is relevant whether or not it can be regarded as a threshold value. It indicates at what laser power a rapid increase in the C/A ratio can be expected. It also allowed us to qualitatively compare the data from the optical tweezers experiments with the data obtained from the calorimetry scans.

5.2.4 Further investigations with Optical Tweezers

To measure forces accurately with OT it is at the moment necessary to use beads as handles. At the powers needed to stably trap a bead (DMPC/DPPC) GUVs deform, which makes it impossible to measure the optical force acting on the membrane. One solution could be to use counter propagating laser beams as in Dimova's paper [74] although the force calibration might be less precise. A rough estimation of the optical force acting on unattached vesicles could be made by using for example the escape method (see section 2.3.1). An other possible view point could be to look at the energy per unit area transmitted to the membrane as did Bar-Ziv et al. [47]. Cherney et al. [44] did an estimation of the gradient force by deriving the free energy lost by trapping the lipid bilayer.

Even if no force measurements could be done in our experiments we were able to extract information about the elastic properties of the membrane. Further investigations would improve our existing results. Using a confocal microscope will make it easier to determine the contour of the vesicle cross-section and give us better data, although the slow image acquisition could give us problems imaging the quick shape fluctuations of the membrane at high laser powers. We will also be able to change the laser power in smaller steps, hence get more data points. This will enlighten the question whether there is indeed a threshold value of the laser power. Some complementary experiments would also be interesting to pursuit. By increasing the laser power slowly we could check if the same heavy fluctuations occur and if so, see if they do at the same laser powers. It would also be nice to get pictures of the whole vesicle deforming, but this requires

the decoupling of the movement of the trapping laser and the movement of the scanning beam. If so, we could measure the area to volume ratio for the whole vesicle and not just look at a cross-section. This is not a trivial problem though. One other thing that could be interesting to think about is the extend of the influence of the viscosity of the surrounding medium on the deformations. Probably this is relevant only if a value is wanted for the optical force exerted on the membrane.

6 Conclusion

In this thesis we tried to give an idea of the effect of near-infrared and infrared optical tweezers on lipid membranes as well as show the temperature dependence of their elastic properties.

The studied GUVs were clearly affected by the optical tweezers. They showed signs of deformation already at quite low laser powers. There as been reports showing that a trapped lipid bilayer is bend into the focus of the trapping laser. This is most probably due to the big difference in dielectric constant between water and the lipid membrane, which is of almost a factor 40. When using moderate laser powers (around 110 mW at the trap focus) and exposure times (under a minute) 1064 nm continuous wave lasers are rather good for optical trapping of biological samples. One should still keep in mind that the highly focused laser beam does have a noticeable effect on the studied sample. Laser-induced heating, although rather small in aqueous solutions and at moderate laser powers, does affect the viscosity of the surrounding media and might affect biological processes. Non-thermal photodamage cannot be fully avoided. As in our experiments, deformation of lipid membranes can occur and a possible stress even on more rigid cellular plasma membranes can't be excluded.

The first step for us in studying the temperature dependence of membrane elasticity was to recognize the existence of a phase transition in lipid bilayers. For the DMPC/DPPC two-component system we studied there is one main phase transition between a solid-ordered and a liquid-disordered phase. We showed this by running differential scanning calorimetry scans of our lipid mixtures. At the transition a change in heat capacity C_p can be measured. This corresponds to a change in enthalpy for the system that carries a lot of thermodynamical information about the melting process of the lipid membrane. We also did some confocal imaging of DMPC/DPPC 50:50 vesicles showing domain formation at temperatures corresponding to the phase transition. Theoretical and experimental work has shown the importance of lateral inhomogeneity for different biological processes like membrane trafficking, for example endo- and exocytosis. By applying an optical force on semi-spherical DMPC/DPPC GUVs using optical tweezers (1064 nm laser) we induced deformations. We quantified these deformations by calculating the circumference to area ratio of a vesicle cross-section. This experiment was performed at different temperatures and for stepwise increasing laser power until the studied vesicle was on the verge of breaking. Two different types of deformation were observed. At moderate laser powers we could only see a change in the circumference of the cross-section, but at high powers heavy fluctuations of the membrane could be seen. By defining a critical power P_c as the transition power between these two deformation regimes, we could compare our data from the tweezer experiments with data from the calorimetry scans. This showed a qualitative correlation between increased heat capacity and a decrease in the laser power needed to deform GUVs. This would suggest an increase in the elasticity of the lipid bilayer at temperatures corresponding to the main phase transition. For a DMPC/DPPC 70:30 mixture the membrane was found to be twice as easy to deform in the phase transition than outside. For DMPC/DPPC 50:50 the corresponding value was 1.33. These results are also

interesting from an experimental point of view. In many published articles little care is given to were in the phase space of the studied system the experiments are carried out, or at least it isn't mentioned. Given the rather drastic changes we observed in the elastic properties of the lipid membrane at the main phase transition, this might at least be interesting to consider. The role of the elasticity increase at the phase transition is not fully understood at the moment, but is most certainly crucial for understanding the function lipid membranes have in all cells.

References

[1] Ole G. Mouritsen, Life - as a matter of fat. The emerging science of lipidomics, Springer Verlag, Heidelberg, 2005, p19-25.

[2] Ole G. Mouritsen, Life - as a matter of fat. The emerging science of lipidomics, Springer Verlag, Heidelberg, 2005, p31-33.

[3] Ole G. Mouritsen, Life - as a matter of fat. The emerging science of lipidomics, Springer Verlag, Heidelberg, 2005, p45-55.

[4] Ole G. Mouritsen, Life - as a matter of fat. The emerging science of lipidomics, Springer Verlag, Heidelberg, 2005, p95-117.

[5] Ole G. Mouritsen, Life - as a matter of fat. The emerging science of lipidomics, Springer Verlag, Heidelberg, 2005, p133-147.

[6] David Boal, Mechanics of the cell, Cambridge University Press, 2002, p139-143.

[7] David Boal, Mechanics of the cell, Cambridge University Press, 2002, p151-168.

[8] E.J.G. Peterman, F. Gittes, C.F. Schmidt. 2003. Laser-induced heating in optical traps. Biophysical journal 84:1308-1316.

[9] C. Leidy, W.F. Wolkers, K. Jørgensen, O.G. Mouritsen, J.H. Crowe. 2001. Lateral organization and domain formation in a two-component lipid membrane system. Biophysical journal 80:1819-1828.

[10] H.M. Seeger, M. Fidorra, T. Heimburg. 2005. Domain size and fluctuations at domain interfaces in lipid mixtures. Macromolecular Symposia 219:85-96.

[11] G. Pabst, H. Amenitsch, D.P.Kharakoz, P. Laggner, M. Rappolt. 2004. Structure and fluctuations of phosphatidylcholines in the vicinity of the main transition. Physical review E 70,021908.

[12] M.I. Angelova, S. Sléau, Ph. Méléard, J.F. Faucon, P. Botherel. 1992. Preparation of giant vesicles by external AC electric fields. Kinetics and applications. Progress in Colloid and Polymer Science 89:127-131.

[13] N. Rodriguez, F. Pincet, S. Cribier. 2005. Giant vesicles formed by gentle hydration and electroformation: A comparison by fluorescence microscopy. Colloids and Surfaces B: Biointerferences 42:125-130.

[14] L.A. Bagatolli, T. Parasassi, E. Gratton. 2000. Giant Phospholipid vesicles: comparison among the whole lipid sample characteristics using different preparation methods. A two photon fluorescence microscopy study. Chemistry and Physics of Lipids 105:135-147.

[15] L. Mathivet, S. Cribier, Ph. Devaux. 1996. Shape change and physical properties of giant phospholipid vesicles prepared in the presence of an AC electric field. Biophysical Journal 70:1112-1121.

[16] L.A. Bagatolli, E. Gratton. 1999. Two-Photon fluorescence microscopy observation of shape changes at the phase transition in phospholipid giant unilamellar vesicles. Biophysical Journal 77:2090-2101.

[17] H. Seeger. 2006. Kinetics of domain formation processes in lipid membranes. Ph.D. thesis. University of Gøttingen.

[18] I. Jelesarov, H.R. Bosshard. 1999. Isothermal titration calorimetry and differential scanning calorimetry as complementary tools to investigate the energetics of biomolecular recognition. Journal of Molecular Recognition 12:3-18.

[19] G. Bruylants, J. Wouters, C Michaux. 2005. Differential scanning calorimetry in life science: Thermodynamics, stability, molecular recognition and application in drug design. Current medicinal chemistry 12:2011-2020.

[20] Biocalorimetry: applications of calorimetry in the biological sciences. Edited by J.E. Ladbury and B.Z. Chowdhry. 1998. John Wiley Sons Ltd, UK.

[21] H. Heerklotz. 2004. The microcalorimetry of lipid membranes. Journal of physics: Condensed matter. 16:R441-R467.

[22] R.N. McElhaney. 1982. The use of differential scanning calorimetry and differential thermal analysis in studies of model and biological membranes. Chemistry and physics of lipids 30:229-259.

[23] M. Fidorra. 2004. Untersuchung des Phasenverhaltens von Membranen durch konfokale Mikroskopie und Kalorimetrie. Diplomarbeit. Gøttingen. p18-22.

[24] Cell biological applications of confocal microscopy, second edition. Edited by B. Matsumoto. 2002. Academic Press, Elsevier Science, USA. p2-13.

[25] Cell biological applications of confocal microscopy, second edition. Edited by B. Matsumoto. 2002. Academic Press, Elsevier Science, USA. p24-45.

[26] Cell biological applications of confocal microscopy, second edition. Edited by B. Matsumoto. 2002. Academic Press, Elsevier Science, USA. p150-164.

[27] Handbook of Biological Confocal Microscopy, third edition. Edited by James B. Pawley. 2006. Springer Science+Business Media, LLC, NY, USA. Printed in Singapore. p1-42.

[28] J. Korlach, P. Schwille, W.W. Webb, G.W. Feigenson. 1999. Characterization of lipid bilayer phases by confocal microscopy and fluorescence correlation spectroscopy. Proceedings of the National Academy of Sciences USA 96:8461-8466.

[29] R. Alvarez-Román, A. Naik, Y.N. Kalia, H. Fessi, R.H. Guy. 2004. Visualization of skin penetration using confocal laser scanning microscopy. European Journal of Pharmaceutics and Biopharmaceutics 58:301-316.

[30] A. Egner, S.W. Hell. 2005. Fluorescence microscopy with super-resolved optical sections(Review). Trends in cell Biology vol:15 nr:4.

[31] M. Fidorra. 2004. Untersuchung des Phasenverhaltens von Membranen durch konfokale Mikroskopie und Kalorimetrie. Diplomarbeit. Gøttingen. p66-67.

[32] http://probes.invitrogen.com/servlets/spectra?fileid=282lip

[33] L. Oddershede, S. Grego, S.F. Norrelykke, K. Berg-Sorensen. 2001. Optical Tweezers: Probing Biological Surfaces. Probe Microscopy 2:129-137.

[34] K.Svoboda, S.M. Block. 1994. Biological applications of optical forces. Annual review of biophysics and biomolecular structure 23:247-85.

[35] K.C. Neuman, S.M. Block. 2004. Optical trapping. Review of scientific instruments vol:75 nr:9.

[36] L. Oddershede, J. Kisbye Dreyer, S. Grego, S. Brown, K. Berg-Sørensen. 2002. The motion of a single molecules, the $\lambda - receptor$, in the bacterial outer membrane. Biophysical Journal 83:3152-3161.

[37] L. Oddershede, H. Flyvbjerg, K. Berg-Serg-Sørensen. 2003. Single-molecule experiment with optical tweezers: improved analysis of the diffusion of the $\lambda - receptor$ in E. Coli's outer membrane. Journal of Physics: Condensed Matter 15:1737-1746.

[38] Biocalorimetry: applications of calorimetry in the biological sciences. Edited by J.E. Ladbury and B.Z. Chowdhry. 1998. John Wiley Sons Ltd, UK. p13.

[39] P. W. M. Van Dijck, A.J. Kaper, H. A. J. Oonk, J. De Gier. 1977. Miscibility properties of binary phosphatidylcholine mixtures. Biochemica et Biophysica Acta 470:58-69.

[40] C. R. Mateo, J-C. Brochon, M. P. Lillo, A. U. Acuna. 1993. Lipid clustering in bilayers detected by the fluorescence kinetics and anisotropy of trans-parinaric acid. Biophysical Journal 65:2237-2247.

[41] S. Marbrey, J. M. Sturtevant. 1976. Investigation of phase transitions of lipids and lipid mixtures by high sensitivity differential scanning calorimetry. Proceedings of the National Academy of Sciences, USA vol 73 No 11:3862-3866.

[42] L. A. Bagatolli, E. Gratton. 2000. A correlation between lipid domain shape and binary phospholipid mixture composition in free standing bilayers: A two-photon fluorescence microscopy study. Biophysical Journal 79:434-447.

[43] T. Heimburg. 1998. Mechanical aspects of membrane thermodynamics. Estimation of the mechanical properties of lipid membranes close to the chain melting transition from calorimetry. Biochemica et Biophysica Acta 1415:147-162.

[44] D. P. Cherney, T. E. Bridges, J. M. Harris. 2004. Optical trapping of unilamellar phospholipid vesicles: Investigation of the effect of optical forces on the lipid membrane shape by confocal-raman microscopy. Analytical chemistry 76:4920-2928.

[45] R. Bar-Ziv, T. Frisch, E. Moses. 1995. Entropic expulsion in vesicles. Physical review letters 75:3481-3484.

[46] J. D. Moroz, P. Nelson, R. Bar-Ziv, E. Moses. 1997. Spontaneous expulsion of giant lipid vesicles induced by laser tweezers. Physical review letters 78:386-389.

[47] R. Bar-Ziv, E. Moses, P. Nelson. 1998.Dynamic excitation in membranes induced by optical tweezers. Biophysical Journal 75:294-320.

[48] E. J. G. Peterman, F. Gittes, C. F. Schmidt. 2003. Laser induced heating in optical traps. Biophysical Journal 84:1308-1316.

[49] Y. Liu, D. K. Cheng, G. J. Sonek, M. W. Berns, C. F. Chapman, B. J. Tromberg. 1995. Evidence for localized cell heating induced by infrared optical tweezers. Biophysical Journal 68:2137-2144.

[50] Y. Liu, G. J. Sonek, M. W. Berns, B. J. Tromberg. 1996. Physiological monitoring of optically trapped cells: Assessing the effects of confinement by 1064-nm laser tweezers using microfluorometry.

[51] S. Wurlitzer, C. Lautz, M. Liley, C. Duschl, Th. M. Fischer. 2001. Micromanipulation of Langmuir-monolayers with optical tweezers. Journal of Physical Chemistry B 105:182-187.

[52] J. Ulander, A. D. J. Haymet. 2003. Permeation across hydrated DPPC lipid bilayers: Simulation of the titrable amphiphilic drug valproic acid. Biophyical Journal 85:3475-3484.

[53] http://en.wikipedia.org/wiki/Dielectric_constant

[54] http://whatis.techtarget.com/definition/0,289893,sid9_gci211945,00.html

[55] http://www.audience-av.com/on_capacitor_dielectric_material.htm

[56] http://www.met.tamu.edu/class/atmo689/lecture5.pdf

[57] http://www.ebi.ac.uk/microarray/biology_intro.html

[58] http://www.estrellamountain.edu/faculty/farabee/biobk/BioBookCELL2.html#Cell%20size%20and%20shape:%20a%20question%20of%20scale

[59] http://en.wikipedia.org/wiki/Red_blood_cell

[60] H. Liang, K. T. Wu, P. Krishnan, T. C. Trang, D. Shin, S. Kimel, M. W. Berns. 1996. Wavelength dependence of cell cloning efficiency after optical trapping. Biophysical Journal 70:1529-1533.

[61] K. König, Y. Tadir, P. Patrizio, M. W. Berns, B. J. Tromberg. 1996. Effects of ultraviolet exposure and near infrared laser tweezers on human spermatozoa. Human Reproduction vol.11 no10:2162-2164.

[62] H. Schneckenburger, A. Hendinger, R. Sailer, M. H. Gschwend, W. S. L. Strauss, M. Bauer, K. Schütze. 2000. Cell viability in optical tweezers: high power red laser diode versus Nd:YAG laser. Journal of Biomedical Optics 5:40-44.

[63] K. C. Neuman, E. H. Chadd, G. F. Liou, K. Bergman, S. M. Block. 1999. Characterization of photodamage to Escherichia coli in optical traps. Biophysical Journal 77:2856-2863.

[64] T. Baumgart, S. Das, W. W. Webb, J. T. Jenkins. 2005. Membrane elasticity in giant vesicles with fluid phase coexistence. Biophysical Journal 89:1067-1080.

[65] T. Baumgart, S. T. Hess, W. W. Webb. 2003. Imaging coexisting fluid domains in biomembrane models coupling curvature and line tension. Nature 425:821-824.

[66] S. Mukherjee, F. R. Maxfield. 2000. Role of membrane organization and membrane domains in endocytic lipid trafficking. Traffic 1:2023-211.

[67] C-H Lee, W-C Lin, J. Wang. 2001. Using differential confocal microscopy to detect the phase transition of lipid vesicle membranes. Optical Engineering 40:2077-2083.

[68] C-H Lee, Y-F Chang, C-H Tsai, P-H Wang. 2005. Optical measurement of the deformation of giant lipid vesicles driven by a micropipette electrode. Langmuir 21:7186-7190.

[69] C-H Lee, W-C Lin, J. Wang. 2001. All-optical measurements of the bending rigidity of lipid-vesicle membranes across structural phase transitions. Physical Review E Vol 64,020901.

[70] C-H Lee, J. Wang. 1997. Noninterferometric differential confocal microscopy with 2-nm depth resolution. Optics Communications 135:233-237.

[71] J. Korlach, C. Reichle, T. Müller, T. Schnelle, W. W. Webb. 2005. Trapping, deformation, and rotation of giant unilamellar vesicles in octode dielectrophoretic field cages. Biophysical Journal 89:554-562.

[72] J-J Foo, K-K Liu, V. Chan. 2003. The thermal effect on a viscously deformed liposome in a laser trap. Annals of Biomedical Engineering 31:354-362.

[73] J-J Foo, K-K Liu, V. Chan. 2004. Viscous drag of deformed vesicles in optical trap: Experiments and simulations. The American Institute of Chemical Engineers Journal 50:249-254.

[74] R. Dimova, B. Pouligny, C. Dietrich. 2000. Pretransitional effects in dimyristoylphosphatidylcholine vesicle membranes: optical dynamometry study. Biophysical Journal 79:340-356.